Evaluation of constant ductility displacement response spectra for near-fault ground motions of the 1999 Chi-Chi earthquake

Konkula Rama Neeraja[1], Faisal Mehraj Wani[2], Chereddy Navyatha[3], Jaya Prakash Vemuri[4]and Chenna Rajaram[5*]

[1]Graduate Student, Department of Civil Engineering, Rajeev Gandhi Memorial College of Engineering and Technology, Nandyal, A.P, INDIA.

[2]Doctoral Student, Mahindra University, Hyderabad, Telangana, INDIA.

[3]Assistant Professor of Civil Engineering, Rajeev Gandhi Memorial College of Engineering and Technology, Nandyal, A.P, INDIA.

[4]Assistant Professor of Civil Engineering, Mahindra University, Hyderabad, Telangana, INDIA.

[5]Associate Professor of Civil Engineering, Rajeev Gandhi Memorial College of Engineering and Technology, Nandyal, A.P, INDIA.

drchenna78@gmail.com, Contact No: +91 90323 45197

Abstract:

This paper investigates the Constant Ductility Displacement Response Spectra (CDDRS) for near-fault ground motions (NFGM) of the 1999 Chi-Chi earthquake. The complex source mechanism was mainly caused by a rupture on the Chelungpu fault that spanned about 100 kilometres. In order to comprehend, a dataset of sixty three NFGM records have been considered to understand the effects of CDDRS due to hanging wall, foot wall, and directivity effects. The CDDRS are generated using SEISMO SIGNAL tool for the selected ground motions. Significant variation is observed in both elastic and inelastic CDDRS for tall buildings due to hanging wall effect. In addition, the variations in inelastic spectra are found to be more prominent due to backward directivity effect. Moreover, the inelastic displacement spectra values for pulse-like

ground motions are much higher than the spectra values associated with non-pulse ground motions.

Keywords: Taiwan; near-fault ground motions; constant ductility response spectra; seismic hazard

Introduction

The 1999 Chi-Chi earthquake (921 earthquake), which was one of the greatest reverse fault earthquakes, occurred in the seismically active area of Taiwan at a depth of 7 km, along the Chelungpu fault, caused by the collision of the Eurasian and Philippine sea plates[1]. The data from recent earthquakes has shown that the ground motion records in the near-fault (NF) region are quite distinct from those obtained from far-field regions[2]. The near-fault ground motion records contain most of the energy in a single or few pulses. Such intense concentration of energy can cause enormous structural damage. The preliminary investigation indicates that around 3000 buildings were collapsed and 6000 buildings were partially damaged during the earthquake[3,4]. In addition to buildings, other structures like bridges, dams, railways, and highways were also suffered severe damage during the earthquake[5]. Damage incurred by several cities adjacent to the fault and the number of buildings affected by the type of structure is depicted in figure 1. Severe damage took place to structures along the length of the fault during the earthquake. The Chelungpu fault trace passed beneath the building in Wu-Feng as shown in figure 1. This rupture produced a vertical displacement of about 2 m through the building. The building was severely damaged due to the differential movement of the fault trace. Another spectacular structural failure is the famous Shihkang dam which was directly uplifted by the fault trace[6]. It was offset by approximately 10 m near its right abutment, primarily due to the dip-slip fault rupture.

In the recent years, displacement-based seismic design has been increasingly implemented as compared to the traditional lateral forces design. Here, the CDDRS plays a crucial role for evaluation of the preliminary design of new structures. Several researchers have examined the influence of ductility requirements for engineering structures under earthquakes[7-11]. Freeman originally developed the Capacity Spectrum Method (CSM) in 1970s, and later Newmark presented the idea of an inelastic response spectrum based on elastic spectra for single-degree-of-freedom systems (SDOF)[10]. Reduction factors were introduced for developing inelastic response spectra for the ground motions from the 1940 El-Centro and 1952 Taft earthquakes[12,13]. Response Reduction Factors (R) were derived for the behavior of strength and stiffness degrading systems[14,15]. The ductility ratio, the period of the structure, and the site conditions were found to have a significant impact on the response spectra[16]. The impact of soil conditions was not thoroughly studied until 1990. Later, the influence of inelastic strength requirements of SDOF considering soil conditions was examined for various ground motion records[17]. Over the years, several empirical equations have been proposed using the constant ductility spectra or damage spectra for the Inelastic Displacement Ratio (IDR), but these studies did not consider pulse-like (PL) ground motions. A recent study performed on the evaluation of constant damage IDR with PL ground motions indicates that these represent greater hazard for structures with strength-degrading behavior[18]. The modern shift towards performance-based earthquake engineering emphasizes strongly the crucial importance of inelastic response spectrum for both SDOF and MDOF systems under PL ground motions[19, 20]. Large pulse period and peak ground velocity greatly increase the inelastic displacement, velocity, and acceleration spectra, indicating that the inelastic response spectra are sensitive to ground motion characteristics and structural hysteresis behavior[21]. Further, to account for the impact of the soil classification and focal mechanism, the study suggests an elastic displacement response spectrum

methodology for near-fault ground motions, that can be used in seismic design since they closely resemble the average elastic displacement response spectra of real earthquake[22]. A constant ductility energy factor spectra were introduced using Gauss–Newton technique for both near and far-fault ground motions[23]. It is shown that significant correlation exists between the computed and estimated energy constant-ductility energy factor spectra. The design of structures as per the contemporary displacement-based methods requires the displacement response spectra for ground motions at the site of interest. Under severe ground motions, the behavior of the structure is inelastic in nature, thus understanding the spectral properties for ductile systems are essential. The structure can be seismically designed to achieve sufficient strength as per these constant ductility response spectra.

The examination of literature indicated that the CDDRS have not been critically examined for NFGMs under various site geology conditions. A key reason could be the limited availability of ground motion records. Since the characteristics of NFGMs are strongly influenced by source rupture processes, they vary significantly from far-field ground motions. Hence, it is essential to examine their constant ductility spectra which can offer insights based on the observed variations from elastic spectra, for various ductility ratios. The main objective of the present study is to investigate the inelastic spectral displacements for various ductility ratios ranging from 1.5 to 3.0 at an interval of 0.5 under NFGMs of the 1999 Chi-Chi earthquake. The study examines the displacement response spectra due to near-fault characteristics and velocity pulses. The study also comprises the variation of CDDRS with respect to site geological conditions.

Strong Motion Dataset of Taiwan

A Peak Ground Acceleration (PGA) of larger than 1 g was recorded on the southern part of the hanging wall and the PGA was gradually decreased to 0.5 g towards the north. Unusually large

values of Peak Ground Velocity (PGV) were also recorded: TCU068 station had a PGV of 383 cm/s and TCU052 station had a PGV of 254 cm/s. The ground motions were recorded at over 150 locations on the hanging wall and 340 locations on the footwall of the Chelungpu fault. In this study, a strong ground motion dataset of 63 NF seismic stations, within 20 km of the Chelungpu fault are collected from the Consortium of Organizations for Strong-Motion Observation Systems (COSMOS) for the 1999 Chi-Chi earthquake. Further, the ground motions are classified according to forward rupture directivity, backward rupture directivity, hanging wall effect and foot wall effect, out of which 6 stations are located on the hanging wall, and 57 stations are located on the footwall as shown in table 1. Figure 2 shows the geographic locations of seismic stations used in the analysis. The site geology of soil is classified according to the National Earthquake Hazards Reduction Program (NEHRP) guidelines based on shear wave velocity at top 30 m. Around 42 sites possess stiff soils in the top 30 m with $V_{s,30}$ varies within 180-360 m/s and 3 sites possess soft soil with $V_{s,30}$ is less than 180 m/s. The amplification factors are high (2.5-2.7) for the sites TCU065 and TCU072 located 10 km apart from the fault. In addition, resonant phenomenon in subsurface soils was observed for the sites located in the NF zones of the 1999 Chi-Chi earthquake.

Methodology to Construct Constant Ductility Displacement Response Spectrum

The current section briefly discusses the methodology to construct the CDDRS for elasto-plastic systems consistent with various levels of the ductility ratio[24-26]. The schematic diagram is shown in figure 3. A step-by-step procedure is described below.

Step-1: The accelerogram $\ddot{u}_g(t)$ is numerically defined.

Step-2: Select the damping ratio, ξ and fundamental natural time period, T_n.

Step-3: Identify the linear system's response *u(t)* and select peak response $u_o(t)$. Calculate the peak force $f_o = ku_o$.

Step-4: Find the elasto-plastic system's response *u(t)*for the same time period and damping ratio. Calculate the yield force, $f_y = \bar{f}_y f_o$ for a range of values ($\bar{f}_y$ = 0.5, 0.25, 0.125). Find the maximum deformation u_m and the corresponding ductility factor (μ) from *u(t)*. Repeat the analysis using other values of $\bar{f}_y$ and, μ.

Step-5: Determine the value, $\bar{f}_y$, for the selected μ, using the results of step-4. If more than one $\bar{f}_y$ value corresponds to a specific value of μ, the largest value of $\bar{f}_y$ is chosen.

Step-6: The spectrum appropriate for the value selected in step 5 is produced by repeating steps 2 through 5 over a range of time periods.

Step-7: For various values of μ, repeat steps 2 through 6.

The analysis considers the displacement ductility μ values ranging from 1.5 to 3.0 with an interval of 0.5, as the typical ranges of μ are in between 3.0 and 6.0[27]. In this analysis, the recently proposed Pulse Indicator (PI) by Kardoutsou is used for classification of PL and NPL ground motions[22]. The results will change if other PI are used for the analysis, as the PI formulation differs for other authors. The PI is characterized based on cross-correlation factor (r) and the equation is as follows.

$$r = \frac{\sum_i \left(f(t_i) - \tilde{f}\right) \mathrm{x}\, g(t_i - t_d) - \tilde{g}}{\left[\sum_i \left(f(t_i) - \tilde{f}\right)^2\right] \mathrm{x} \left[\sum_i \left(g(t_i - t_d) - \tilde{g}\right)^2\right]} \quad (1)$$

Where $\tilde{f}$ and $\tilde{g}$ being the mean values of the functions *f* and *g*, respectively. t_d is the time delay parameter at which the pulse starts.

Results and Discussion

Characteristics of Near-Fault Ground Motions

Large pulse amplitude and long pulse duration are the key features in the velocity records of NFGMs. These observations are substantially different from far-field ground motions as illustrated in figure 4. Further, most of the energy content is confined in a single or a few pulses. These pulses can also be due to the *directivity effect* and the *fling effect*. In this section, CDDRS are examined for hanging wall, footwall, forward and backward rupture directivity for various ductility ratios (μ = 1.5, 2.0, 2.5, 3.0) are shown in figure 5. As, the spectral displacements vary for each ground motion record at a particular fundamental period of the structure, it is essential to use the mean values. Further, the ground motions are classified as either PL or NPL using different schemes, to evaluate the CDDRS for obtaining the structural response.

Hanging wall: A set of six stations are situated on the hanging wall side of the Chelungpu fault. The spectra of ground motions from these stations, for various ductility ratios, are compared with the elastic displacement spectrum. A variation is observed between inelastic spectra of different ductility ratios. No significant variation is observed between the elastic and the inelastic spectra till T_n reaches 2.35 s. and significant variation is observed beyond T_n = 2.35 s (i.e., for tall buildings).

Footwall: A set of fifty-seven stations are situated on the footwall side of the Chelungpu fault. The spectra of ground motions from these stations, for various ductility ratios, are compared with the elastic displacement spectrum. It has been observed that there is insignificant variation between inelastic displacement spectra of various ductility ratios and the elastic displacement spectrum on footwall.

Forward rupture directivity: A set of fifty-three stations are located on the forward rupture directivity side of the Chelungpu fault. The spectra of ground motions from these stations, for various ductility ratios, are compared with the elastic displacement spectrum. There is no

significant variation in the inelastic spectra obtained for different ductility ratios and the elastic spectrum. It indicates that the forward rupture directivity has no substantial effect on the elastic and the inelastic displacement spectra.

Backward rupture directivity: A set of ten stations are located on the backward rupture directivity side of the Chelungpu fault. The spectra of these stations, for various ductility ratios, are compared with the elastic displacement spectrum. It is observed that there is a significant variation between the inelastic spectra of different ductility ratios and the elastic spectrum. No significant difference is observed between inelastic spectra with various ductility ratios. The average elastic and inelastic spectra for various ductility ratios are shown in figure 6.

Velocity Pulse Parameters

The ground motion records are classified as *PL*, *NPL* and *ambiguous* using the approach proposed by Kardoutsou[28]. The current study uses Kardoutsou PI for pulse classification. According to this approach, if the PI values are greater than 0.65 the ground motions are termed as *PL*. If PI is less than 0.55, such ground motions are termed as *NPL*. If the value of PI lies between 0.55 and 0.65, the ground motions are termed as *ambiguous.* A sharp velocity pulses exhibit high amplitude and long pulse duration may lead to significant damage to engineered structures. The current study examines the effect of pulse period and pulse identification on CDDRS.

Pulse period: Four different pulse periods 1.2 s, 1.8 s, 3.3 s, and 3.9 s are considered for the study. No substantial change in inelastic response spectra is observed for the fundamental time period, T<1.3 s and significant change is observed beyond T=1.3 s. This indicates that the velocity pulse periods can influence the inelastic response spectra for high-rise buildings. Figure 7 shows the inelastic displacement spectra.

Pulse identification: The inelastic displacement spectra are drawn for ductility ratios of 1.5, 2.0, 2.5, and 3.0. Since the ground motion data is large, an average inelastic spectrum is considered for all μ values. It is observed that the inelastic displacement spectra values for PL ground motions are twice the values observed for NPL ground motions. No significant deviation is observed in the inelastic displacement spectra of PL and NPL ground motions for various ductility values shown in figure 7. However, a deviation is observed in ambiguous ground motions for T > 2.5 s. The results may vary with other definitions of PI. For this purpose, a comparison has also been performed using other PIs proposed by various authors. Figure 8 represents the inelastic displacement spectra for PL, and NPL proposed by various researchers for ductility ratio $\mu = 3.0$[29-31, 27]. It is observed that the PL spectra, based on Baker and Panella PI's, lead to higher inelastic spectral displacements due to a higher PI values defined by both researchers. According to Baker and Panella, the PL ground motions are those for which the PI values are greater than 0.85, and 0.7, respectively. It is also observed that the NPL spectra based on Baker's PI, lead to lower displacement values. These observations indicate the importance of PL and NPL ground motions for developing CDDRS.

Effect of Closest Distance from the fault, R

Various distances: To study the inelastic displacement response spectra for various closest distances from the fault, a plot is drawn as shown in figure 9. High displacement values are observed for the closest distance to fault, R=1.1 km till T < 2.3 s. No significant change is observed in spectra for T < 2.3 s for higher distance values. Beyond this range, the displacement values are considerably high.

Same distance: Two seismic stations located at the same closest distance to the fault, i.e.13.3 km are examined. While one station is situated on a hanging wall, the other station is situated on the footwall. The inelastic displacement spectra are developed for ground motions

from the two stations with different ductility ratios. From the results, it is observed that the station located on the hanging wall leads to larger displacement values as compared to the station located on the footwall, as shown in figure 9. In the case of hanging walls, the seismic energy gets trapped on the wedge portion resulting in higher acceleration values.

Effect of site classification

In the 1999 Chi-Chi earthquake, most recording stations were situated on soil. The soil behavior was non-linear in the NF region[32]. Since detailed borelog data and subsurface soil properties are often not available for every site, sites are usually classified into various classes, using information from a combination of sources, i.e. geological maps, digital elevation models, borelog data, shear wave velocity and response spectra from historical ground motion data. The site class description used in the present study is based on geological studies of the region reported by Lee[33].

From figure 10, no significant change is observed in inelastic displacement spectra for various μ values for T_n is less than 1.0 s (for low-rise and mid-rise buildings) and considerable change is observed for T_n beyond 1.0 s. For higher site classification, the inelastic displacement values change abnormally for T_n beyond 1.0 s due to nonlinearity of soil. Overall, the results obtained from various site classifications indicate the NFGMs have a distinct impact in the various CDRS. The results thereby provide an insight into the general evaluation of CDDRS for NFGMs.

CDDRS with different authors

A comparison is done between CDDRS obtained from the *Seismosignal* and *Open Seismo MATLAB* application tools for validation purposes[34, 35]. The present study uses the commercial *Seismosignal* tool for developing CDDRS at four seismic stations WNT, CHY028, CHY080,

TCU065 that are located 2.2 km, 8.7 km, 3.1 km, 2.5 km from the Chelungpu fault respectively. A key reason for the selection of the tool is that it is an easy to use, reliable and the most widely used tool by various researchers worldwide. For the purpose of validation, the derived results are compared with the *Open-Seismo MATLAB* tool developed by George Papazafeiropoulas[36]. It is known that conventional time integration algorithms are incorporated in *Seismosignal* to calculate the dynamic response. However, the *Open-Seismo MATLAB* tool computed the CDDRS through nonlinear dynamic analyses of elasto-plastic hysteretic systems, rather than simplified approaches. The target ductility $\mu = 3.0$ is considered in the analysis. No significant change in inelastic spectra is observed using both application tools. A slight variation is observed for the station CHY028 at periods between fundamental natural periods T = 2.25 s and 3.0 s. Though the percentage of error is negligible, a slight variation is observed between spectra using both application tools as shown in figure 11. The variation in the results is due to the following:

- *Seismosignal* tool uses conventional time integration algorithms and *Open-Seismo MATLAB* uses advanced time integration algorithms to minimize the errors for certain cases.
- Elasto-plastic bilinear kinematic hardening constitutive models for Single Degree of Freedom (SDOF) systems are implemented in *Open-Seismo MATLAB.*
- *Open-Seismo MATLAB* uses Generalized Single Step Single Solve (GSSSS) algorithms for calculating the displacement of the SDOF systems and *Seismosignal* tool uses Newmark's family algorithms.

Conclusions

The structural damage in near-fault regions was high and it was reported that unreinforced masonry structures and reinforced concrete structures were destroyed in Taichung and Nantou during the 1999 Chi-Chi earthquake. Literature on constant ductility spectra for near-fault

ground motions is limited due to scarcity of near-fault data recorded in major earthquakes. The current study presents CDDRS from various ground motion records of the 1999 Chi-Chi earthquake due to near-fault characteristics. Some salient conclusions are now discussed.

- The elastic and inelastic CDDRS have no remarkable effect across all periods of buildings due to the ground motions located on foot wall of the Chelungpu fault. On other hand, significant variations are observed in both elastic and inelastic CDDRS for tall buildings (T_n> 2.35 s) due to hanging wall effect. Reconnaissance studies also indicate that greater structural damage was observed on the hanging wall side.
- Notable changes are observed in the inelastic CDDRS due to backward rupture directivity, but no effect is observed on the CDDRS due to forward rupture directivity.
- Inelastic CDDRS for PL ground motions are twice than NPL ground motions due to large amplitude and period of ground motions.
- Further, the results obtained from various site classifications indicate the near-fault ground motions have a significant and distinct impact in the CDRS. Both low-rise and mid-rise buildings, no significant change are observed in the inelastic CDRS for different ductility values of mid-rise buildings (T_n< 1.0 s), and significant variation is observed for high-rise buildings (T_n> 1.0 s).
- Finally the results are validated using two softwares and it is observed that the results are to be within a reasonable level of accuracy.

The CDDRS evaluation does not incorporate the influence arising from the various orientations of ground motion records.

Conflict of Interest

The author(s) declare that there is no conflict of interest regarding this article's research, authorship, and/or publication.

References

1. Shin, T.C. and Teng, T.L., An overview of the 1999 Chi-Chi, Taiwan, earthquake. *Bulletin of the seismological society of America*, 2001, **91**(5), 895-913.
2. Alavi, B. and Helmut, K., Effects of near-fault ground motions on frame structures. Stanford: John A. Blume Earthquake Engineering Center, USA, 2001.
3. Chen, C. C. Huang, C. T. Cherng, R. H. and Jeng, V., Preliminary investigation of damage to near fault buildings of the 1999 Chi-Chi earthquake. *Earthquake Engineering and Engineering Seismology*, 2000, **2**(1), 79-92.
4. Tsai, K. C. Hsiao, C. P. and Bruneau, M., Overview of building damages in 921 Chi-Chi earthquake. *Earthquake Engineering and Engineering Seismology*, 2000, **2**(1), 93-108.
5. Su, N. Lin, T. D. and Chai, H. W., Damage to structures and buildings from the Chi-Chi (Taiwan) earthquake. *Proceedings of the Institution of Civil Engineers-Structures and Buildings*, 2002, **152**(1), 51-56.
6. Bray, J.D., Developing Mitigation Measures for the Hazards Associated with Earthquake Surface Fault Rupture, *Seismic Fault-induced Failures*, 2001, 55-80.
7. Veletsos, A. S. Newmark, N. M. and Chelapati, C. V., Deformation spectra for elastic and elastoplastic systems subjected to ground shock and earthquake motions. *Proc. 3rd world conference on earthquake engineering, NewZealand*, 1965, 663-682.
8. Newmark, N. M. and Hall, W. J., Seismic design criteria for nuclear reactor facilities. *Proc. 4th World conference on Earthquake Engineering, Santiago*, 1969, 37-50.

9. Murakami, M. and Penzien, J., Nonlinear response spectra for probabilistic design of reinforced concrete structures. *Proc. 6th World Conference on Earthquake Engineering, New Delhi*, 1977, 1046-1051.
10. Newmark, N. M. and Riddle, R., Inelastic spectra for seismic design. *Proc. 7thWorld Conference on Earthquake Engineering, Istanbul*, 1980, 129-136.
11. Lai, S. S. P. and Biggs, J. M., Inelastic response spectra for aseismic building design. *Journal of the Structural Division*, 1980, **106**(6), 1295-1310.
12. Saini, S. S., Design spectrum for epicentral earthquakes. *Proc. 2nd International Conference on Computer Aided Analysis and Design in Civil Engineering, University of Roorkee, India*, 1985, 41-47.
13. Pal, S. Dasaka, S. S. and Jain, A. K., Inelastic response spectra. *Computers and structures*, 1987, **25**(3), 335-344.
14. Riddell, R. Hidalgo, P. and Cruz, E., Response modification factors for earthquake resistant design of short period buildings. *Earthquake spectra*, 1989, **5**(3), 571-590.
15. Krawlinker, H. and Nassar, A., Seismic design based on ductility and cumulative damage demands and capacities. In: Nonlinear seismic analysis of reinforced concrete buildings. CRC Press, New York, USA, 1992, 27–47.
16. Chopra, A. K. and Goel, R. K., Capacity-demand-diagram methods based on inelastic design spectrum. *Earthquake Spectra*, 1999, **15**(4), 637-656.
17. Miranda, E., Nonlinear response spectra for earthquake resistant design. *Proc. 10th World Conference on Earthquake Engineering*, Madrid, Spain. 1992.
18. Wei-Ping, W. Chang-Hai, Z. Shuang, L. Zhiwang, C. Li-Li, X., Constant damage inelastic displacement ratios for the near-fault pulse-like ground motions, *Engineering Structures*, 2014, **59**, 599-607.

19. Changhai, Z. Weiping, W. Duofa, J. Shuang, L., The influences of aftershocks on the constant damage inelastic displacement ratio. *Soil Dynamics and Earthquake Engineering*, 2015, **79,** 186-189.
20. Foteini, K. George, H., Constant-ductility inelastic displacement, velocity and acceleration ratios for systems subjected to simple pulses, *Soil Dynamics and Earthquake Engineering*, 2020, **131,** 106027.
21. Dong, H. Han, Q. Du, X. Cheng, S. He, H., Inelastic response spectra of self-centering structures with the flag-shaped hysteretic response subjected to near-fault pulse-type ground motions. *Earthquake Spectra*. 2021, **37**, 2767-2794.
22. Maniatakis, C.A. Spyrakos, C.C., A new methodology to determine elastic displacement spectra in the near-fault region. *Soil Dynamics and Earthquake Engineering*, 2012, **35**, 41-58.
23. Ucar, T. Merter, O., Predictive Model for Constant-Ductility Energy Factor Spectra of Near- and Far-Fault Ground Motions Based on Gauss–Newton Algorithm. *Journal of Earthquake Engineering*, 2022, **15**, 7689-7714.
24. Yi, W.J. Zhang, H.Y. Kunnath, S.K. Probabilistic constant-strength ductility demand spectra. *Journal of structural engineering*, 2007, **133**, 567-575.
25. Colunga, A.T., Displacement ductility demand spectra for the seismic evaluation of structures. *Engineering Structures*, 2001, **23**, 1319-1330.
26. Madhu, G.H. Gupta, V.K., Scaling of constant-ductility residual displacement spectrum. *Earthquake Engineering & Structural Dynamics*, 2020, **49**, 215-233.
27. Alfredo, R.S. Edén, B. Juan, B. Federico, V.B. Mario, D. and Llanes, T., Energy Dissipation and Local, Story, and Global Ductility Reduction Factors in Steel Frames under Vibrations Produced by Earthquakes, *Shock and Vibration*, 2018, 9713685.

28. Kardoutsou, V. Taflampas, I. and Psycharis, I. N., A new pulse indicator for the classification of ground motions. *Bulletin of the Seismological Society of America*, 2017, **107**(3), 1356-1364.
29. Baker, J. W., Quantitative classification of near-fault ground motions using wavelet analysis. *Bulletin of the seismological society of America*, 2007, **97**(5), 1486-1501.
30. Panella, D. S. Tornello, M. E. and Frau, C. D., A simple and intuitive procedure to identify pulse-like ground motions. *Soil Dynamics and Earthquake Engineering*, 2017, **94**, 234-243.
31. Zhai, C. Chang, Z. Li, S. Chen, Z. and Xie, L., Quantitative identification of near-fault pulse-like ground motions based on energy. *Bulletin of the Seismological Society of America*, 2013, **103**(5), 2591-2603.
32. Pavlenko, O.V., Characteristics of soil response in near-fault zones during the 1999 Chi-Chi, Taiwan, Earthquake. *Pure and applied geophysics*, 2008, **165**(9), 1789-1812.
33. Lee, C.T. Cheng, C.T. Liao, C.W. and Tsai, Y.B., Site classification of Taiwan free-field strong-motion stations. *Bulletin of the Seismological Society of America*, 2001, **91**(5), 1283-1297.
34. SeismoSoft, Seismo Signal A computer program for signal processing of strong-motion data, Pavia, Italy, 2021.
35. The MathWorks, Inc., MATLAB Release 2020b Natick, Massachusetts, United States of America, 2020
36. Papazafeiropoulos, G. and Plevris, V., Openseismomatlab: A new open-source software for strong ground motion data processing. *Heliyon*, 2018, **4**(9), 784.

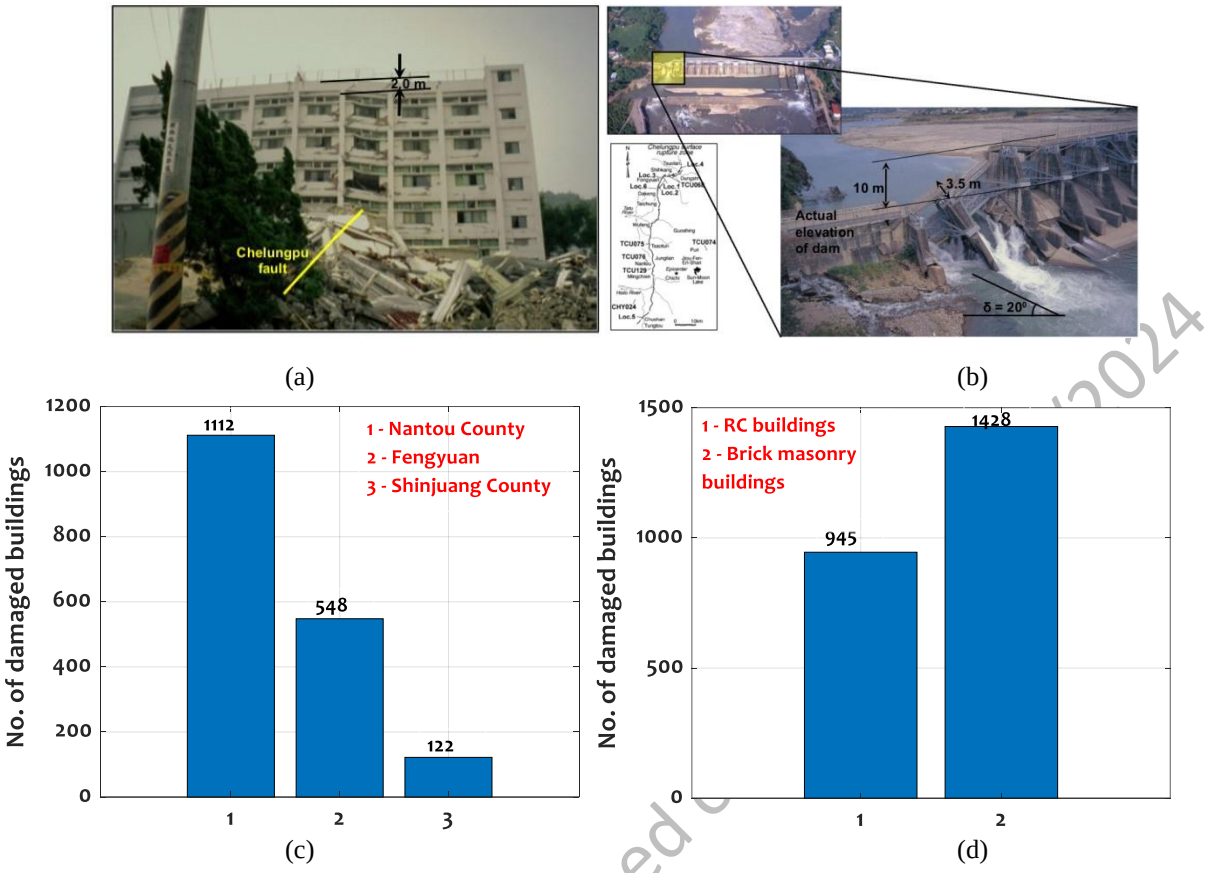

Figure 1. Damage of structures due to surface rupture and statistics of the damaged buildings in affected areas during 1999 Chi-Chi earthquake (a) the Chelungpu fault passed beneath this apartment building in Wu Feng (Photo Courtesy: K. Kelson). (b) view to the east of surface fault rupture through Shihkang Dam (Photo Courtesy: J.D. Bray). (c) number of damaged buildings in affected areas of Taiwan, and (d) number of damaged RC and brick masonry buildings.

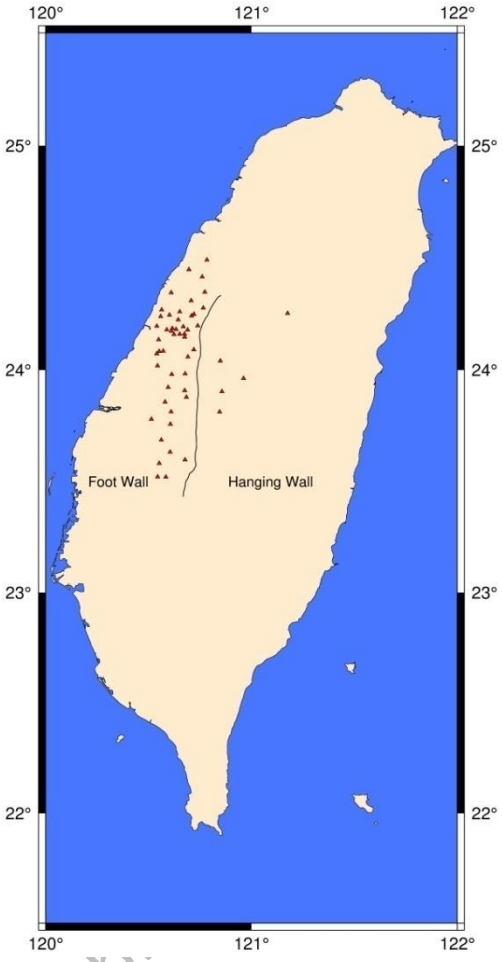

388

389 Figure 2. Location of seismic stations considered in the analysis

390

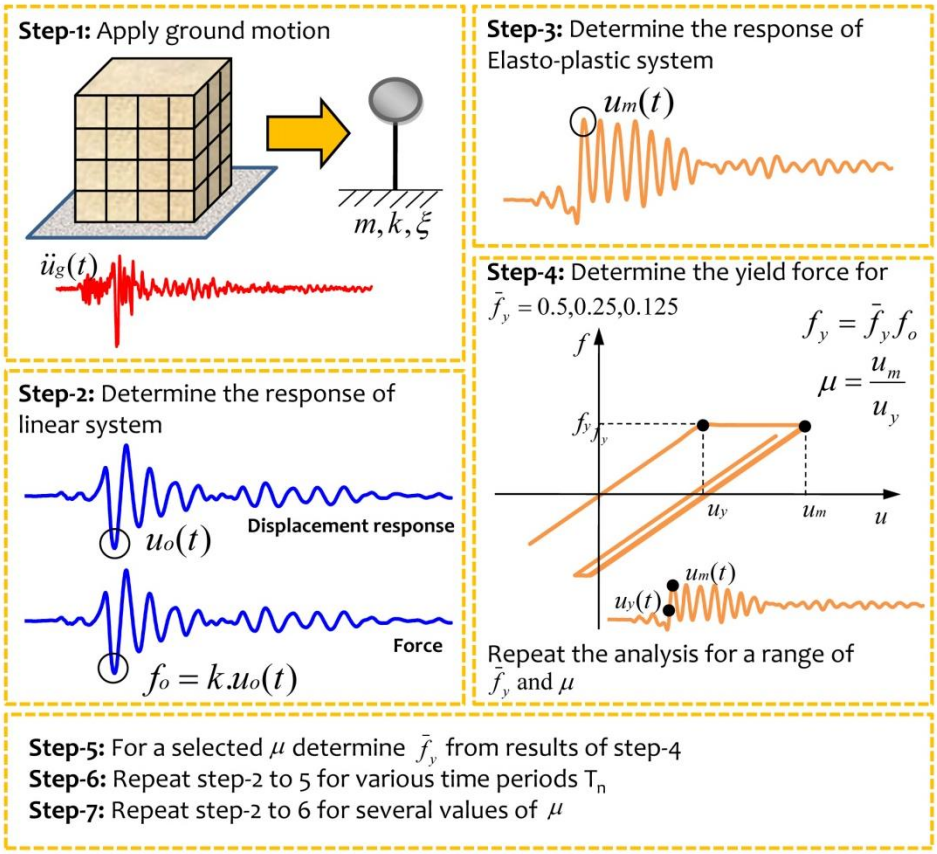

Figure 3. Schematic diagram of constructing constant ductility response spectrum

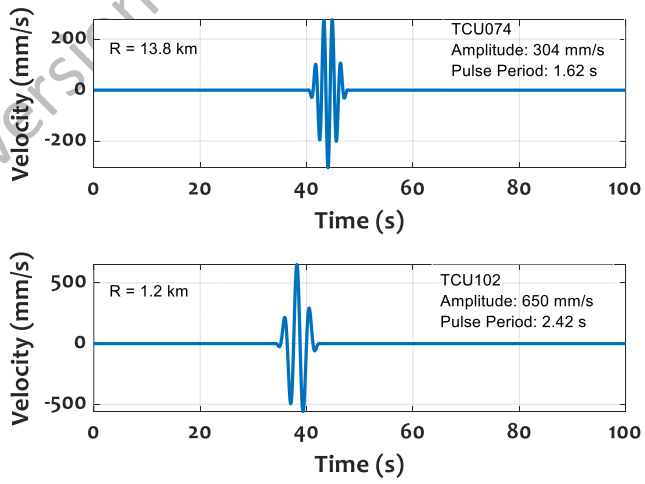

Figure 4. Velocity pulses at two different stations

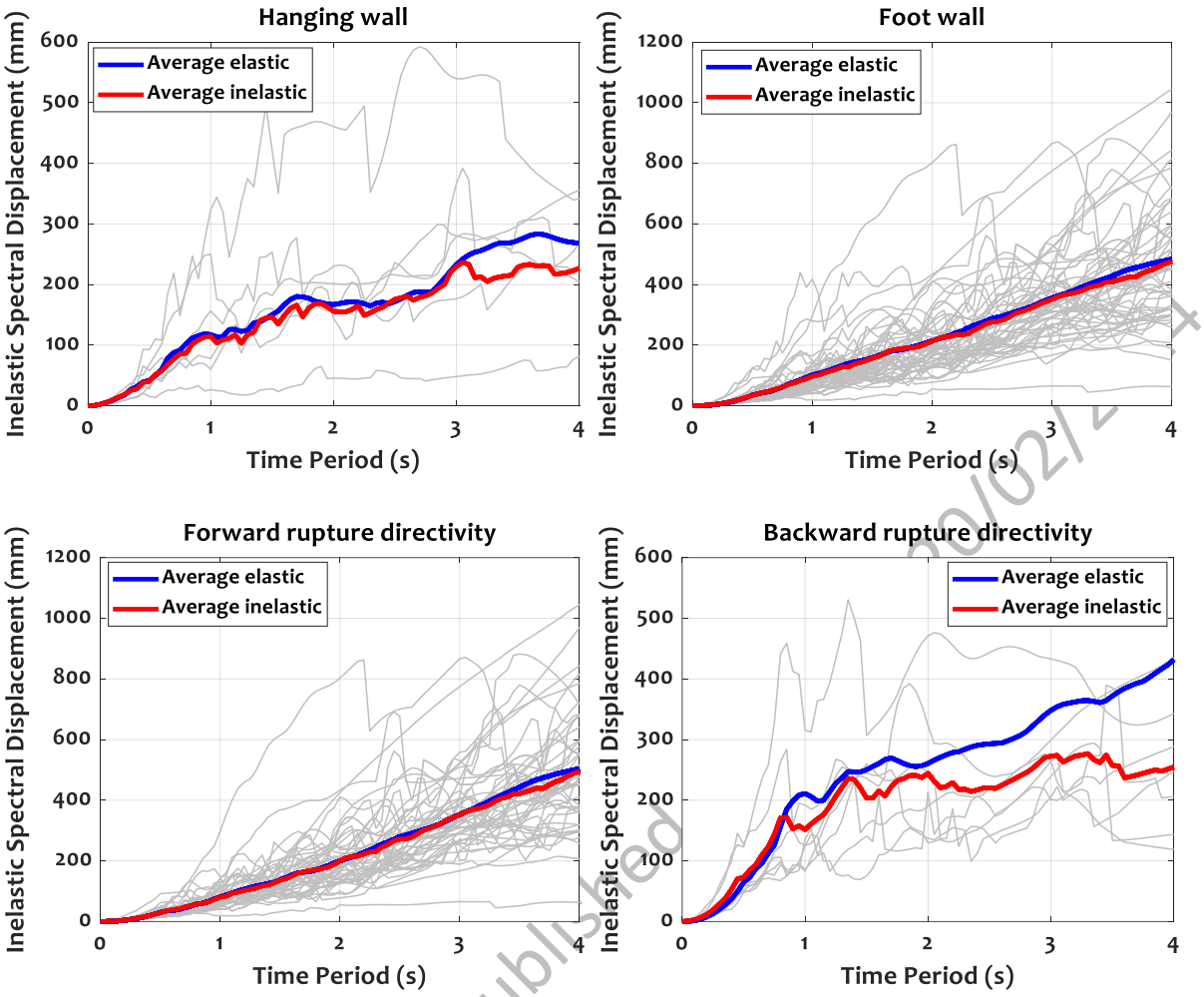

Figure 5. Inelastic spectral displacements for hanging wall, foot wall, forward and backward rupture directivity of near- fault ground motions during 1999 Chi-Chi earthquake (μ=3.0). The average elastic spectrum and inelastic spectrum are represented with blue and red colors respectively.

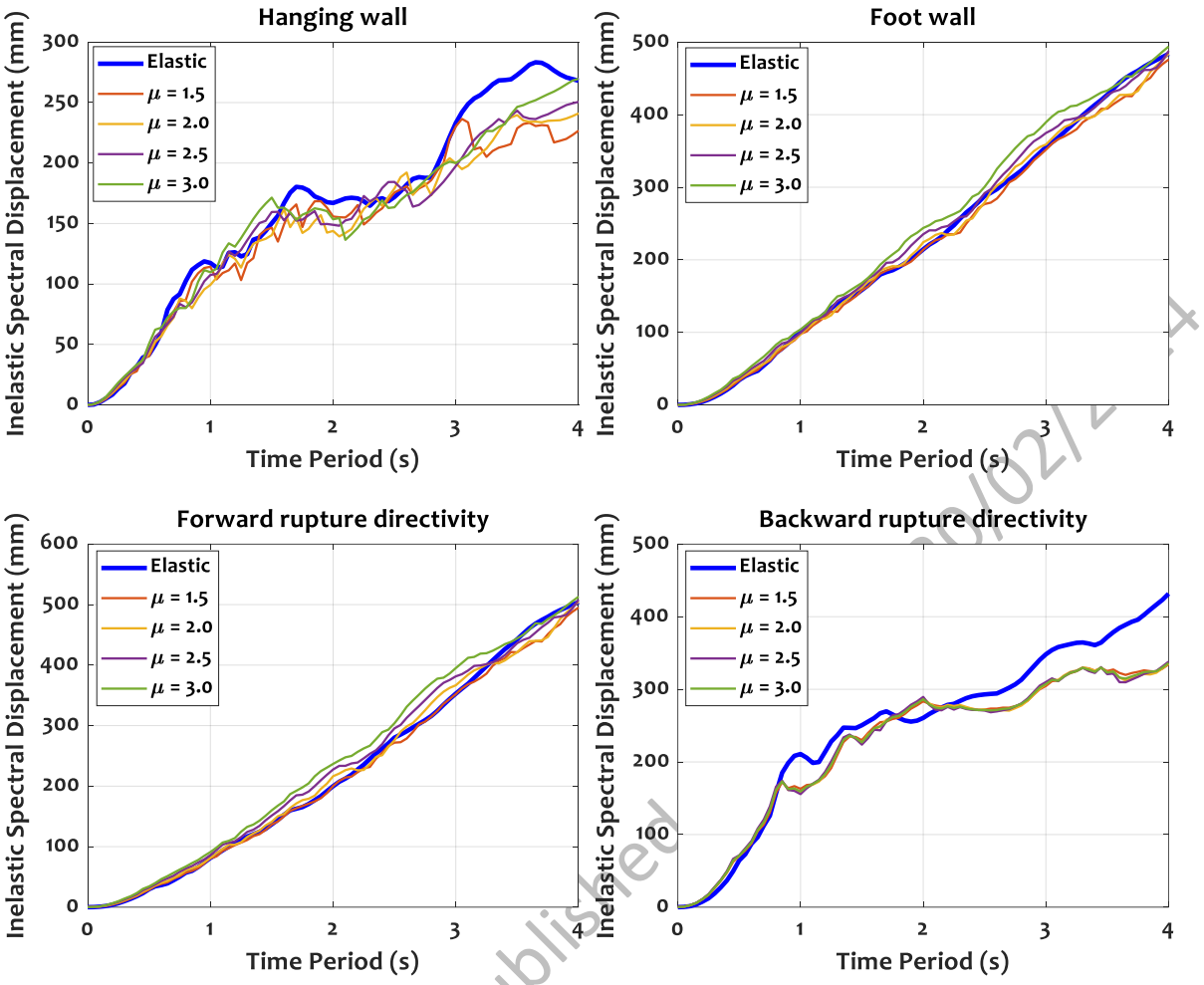

Figure 6. Mean of elastic and inelastic spectral displacements for different ductility ratios

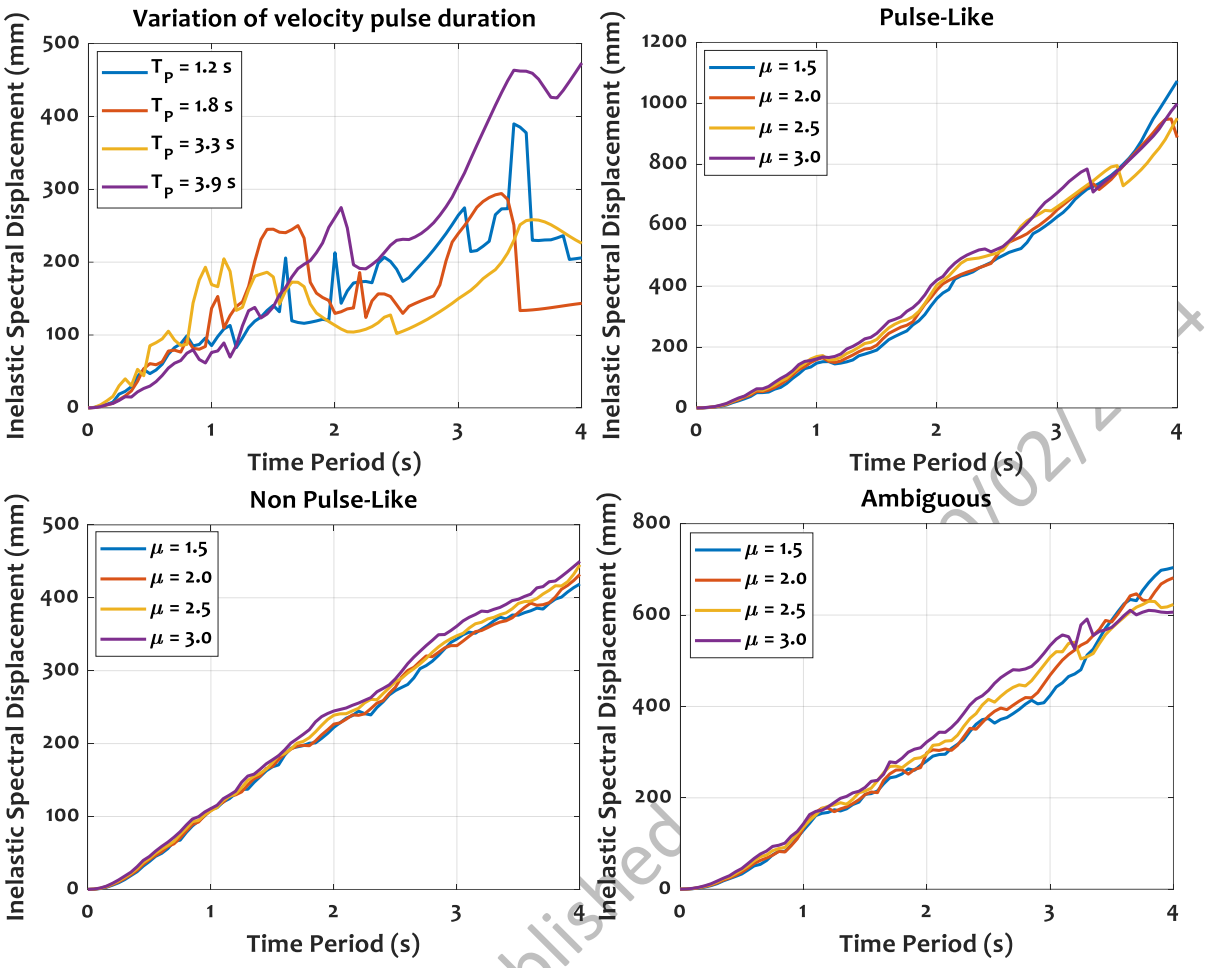

Figure 7. Comparison of displacement spectra for various pulse periods and various ductility ratios of pulse-like, non pulse-like, and ambiguous ground motions of the 1999 Chi-Chi earthquake.

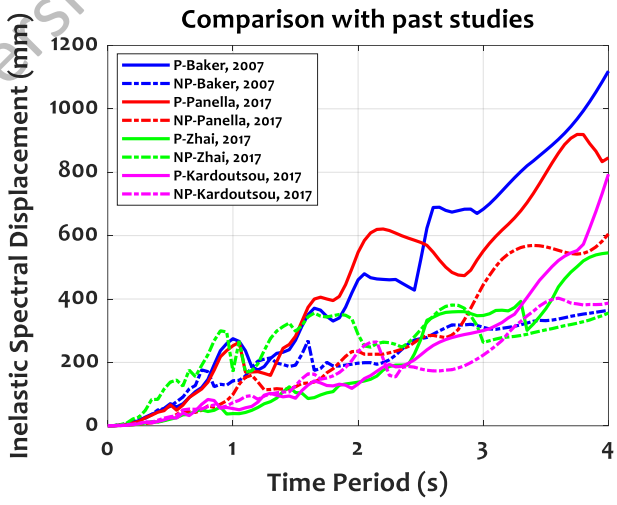

Figure 8. Classification of inelastic displacement spectra for pulse-like and non-pulse like ground motions defined by various researchers (μ=3.0). The current study uses Kardoutsou PI for pulse classification.

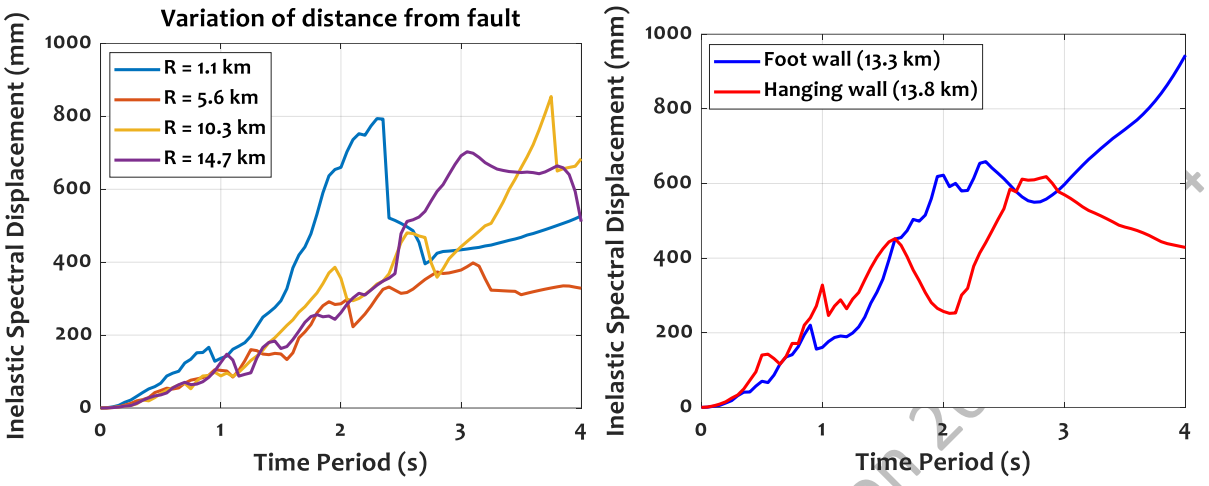

Figure 9. Comparison of inelastic displacement spectra with the stations located at different distances and same distance from fault (μ=3.0)

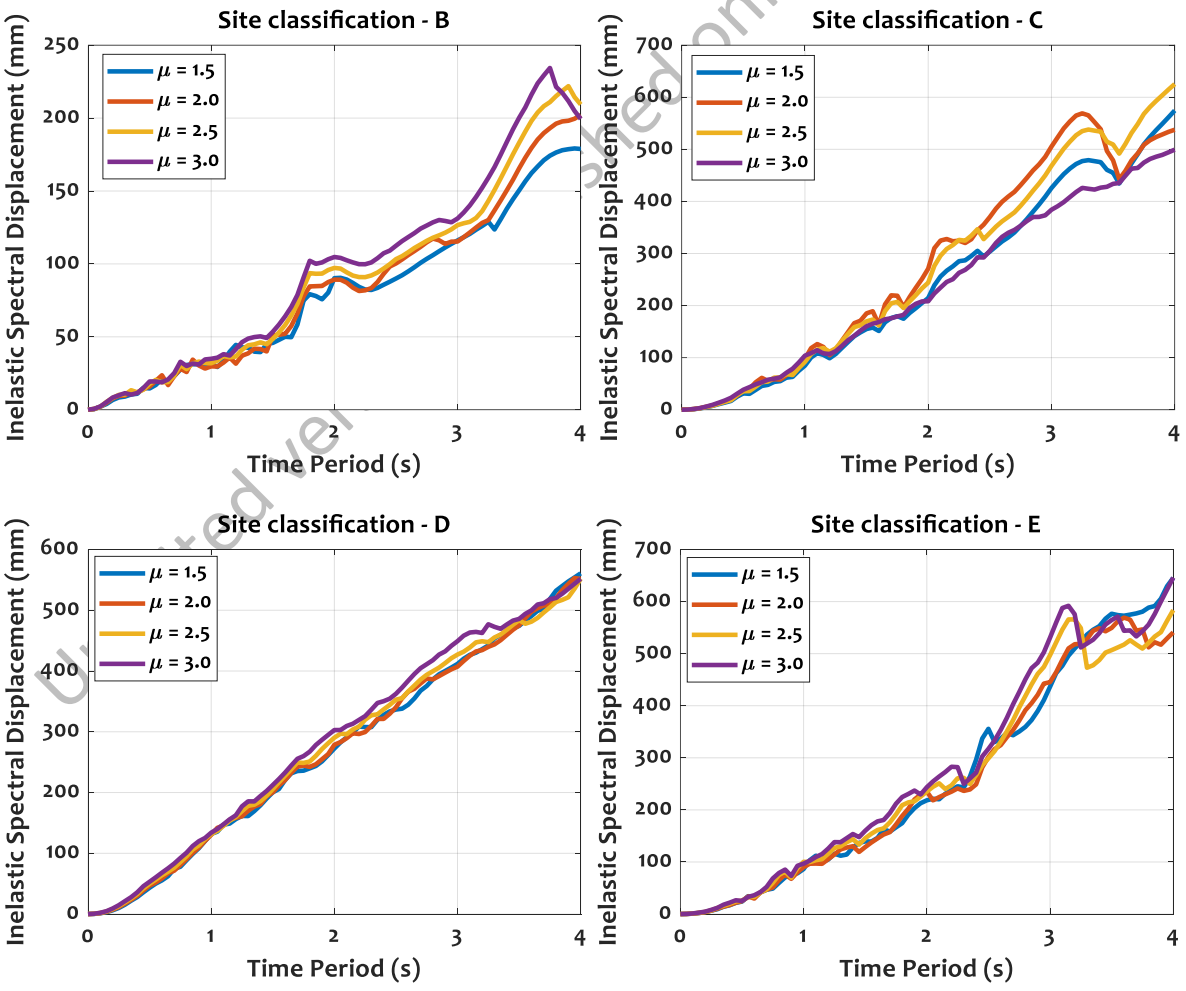

Figure 10. Comparison of inelastic displacement spectra with various site classifications B, C, D, and E for various ductility ratios

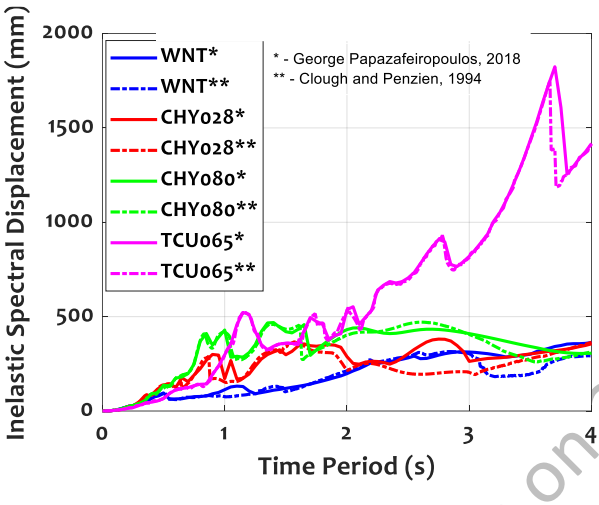

Figure 11. Comparison of inelastic displacement spectra with various methods proposed by different authors

439 Table 1.Details of seismic stations of the 1999 Chi-Chi earthquake occurred on 20 September
440 1999 with a magnitude of Mw7.6 (latitude: 23.86, longitude: 120.80) *(Data Source: COSMOS)*

SNo	Station Name	Station Lat.	Station Long.	Closest Distance to Fault (km)	Epicentral Distance (km)	Site Geology	Near-Fault Characteristics			
							Hanging Wall	Foot Wall	Forward Rupture	Backward Rupture
1	TCU078	23.81	120.85	8.30	7.40	D	*		*	
2	TCU089	23.90	120.86	12.80	7.95	C	*		*	
3	WNT	23.88	120.68	2.20	12.94	D		*	*	
4	TCU076	23.91	120.68	3.20	14.71	D		*	*	
5	TCU075	23.98	120.68	3.40	19.16	D		*	*	
6	TCU122	23.81	120.61	9.20	21.72	D		*	*	
7	TCU074	23.96	120.96	13.80	21.27	D	*		*	
8	TCU072	24.04	120.85	7.90	20.76	D	*		*	
9	TCU138	23.92	120.60	11.30	23.67	D		*	*	
10	TCU116	23.86	120.58	12.50	24.33	E		*	*	
11	CHY024	23.76	120.61	9.30	24.33	D		*	*	*
12	TCU120	23.98	120.61	9.90	24.62	C		*	*	
13	TCU065	24.06	120.69	2.50	25.10	D		*	*	
14	TCU067	24.09	120.72	1.10	27.11	D		*	*	
15	CHY025	23.78	120.51	18.80	32.97	E		*	*	
16	CSMIP	23.69	120.56	13.30	32.67	D		*		*
17	CHY101	23.69	120.56	13.30	32.67	D		*		*
18	TCU123	24.02	120.54	17.10	33.40	D		*	*	
19	CHY080	23.60	120.68	3.10	32.18	---		*		*
20	CHY028	23.63	120.61	8.70	33.28	D		*		*
21	TCU063	24.11	120.61	10.30	34.64	D		*	*	
22	TCU055	24.14	120.66	5.60	34.61	D		*	*	
23	TCU109	24.08	120.57	14.70	35.53	D		*	*	
24	TCU082	24.15	120.68	4.50	34.70	D		*	*	
25	TCU	24.15	120.68	4.50	34.70	D		*	*	
26	TCU106	24.08	120.55	16.70	37.00	D		*	*	
27	TCU107	24.07	120.54	17.80	37.21	D		*	*	
28	TCU054	24.16	120.68	4.60	36.15	D		*	*	
29	TCU051	24.16	120.65	7.00	37.12	D		*	*	
30	TCU049	24.18	120.69	3.30	37.40	D		*	*	
31	TCU056	24.16	120.62	9.80	38.45	D		*	*	
32	TCU052	24.20	120.74	1.80	38.08	D	*		*	
33	CHY074	23.51	120.80	14.40	38.88	C	*			*
34	CHY029	23.61	120.52	16.40	41.65	C		*		*

35	TCU053	24.19	120.67	5.50	39.73	D		*	*	
36	TCU050	24.18	120.63	8.90	40.12	D		*	*	
37	TCU057	24.17	120.61	11.20	40.56	C		*	*	
38	TCU061	24.14	120.55	17.20	41.31	D		*	*	
39	CHY006	23.58	120.55	14.50	41.38	D		*		*
40	TCU100	24.19	120.62	10.80	41.51	C		*	*	
41	TCU048	24.18	120.59	13.40	42.50	C		*	*	
42	TCU060	24.22	120.64	8.10	43.98	D		*	*	
43	TCU101	24.24	120.71	1.90	43.54	D		*	*	
44	CHY035	23.52	120.58	15.20	44.71	D		*		*
45	TCU102	24.25	120.72	1.20	44.05	D		*	*	
46	TCU070	24.20	120.54	18.40	47.08	C		*	*	
47	CHY034	23.52	120.54	18.20	47.11	D		*		*
48	TCU068	24.28	120.77	3.00	46.43	D		*	*	
49	TCU136	24.26	120.65	7.50	47.33	C		*	*	
50	TCU104	24.25	120.60	12.50	48.06	C		*	*	
51	TCU105	24.24	120.56	16.80	49.80	C		*	*	
52	TCU103	24.31	120.71	2.40	50.94	D		*	*	
53	TCU059	24.27	120.56	16.50	52.35	D		*	*	
54	TCU087	24.35	120.77	3.40	54.23	C		*	*	
55	TCU064	24.35	120.61	12.20	57.84	D		*	*	
56	TCU088	24.25	121.18	13.20	60.40	B	*		*	
57	NSY	24.42	120.76	9.10	61.86	C		*	*	
58	TCU128	24.42	120.76	9.10	61.86	C		*	*	
59	TCU036	24.45	120.70	12.70	66.32	D		*	*	
60	TCU040	24.45	120.64	15.00	67.78	E		*	*	
61	TCU046	24.46	120.85	16.50	66.80	B		*	*	
62	TCU039	24.49	120.78	17.50	70.11	C		*	*	
63	TCU038	24.49	120.66	18.20	71.59	D		*	*	

441

442

443

444

Evaluation of Constant Ductility Displacement Response Spectra for Near-Fault Ground Motions of the 1999 Chi-Chi Earthquake

Konkula Rama Neeraja[1], Faisal Mehraj Wani[2], Chereddy Navyatha[3], Jaya Prakash Vemuri[4]and Chenna Rajaram[5*]

[1]**Graduate Student, Department of Civil Engineering, Rajeev Gandhi Memorial College of Engineering and Technology, Nandyal, A.P, INDIA.**

[2]**Doctoral Student, Mahindra University, Hyderabad, Telangana, INDIA.**

[3]**Assistant Professor of Civil Engineering, Rajeev Gandhi Memorial College of Engineering and Technology, Nandyal, A.P, INDIA.**

[4]**Assistant Professor of Civil Engineering, Mahindra University, Hyderabad, Telangana, INDIA.**

[5]**Associate Professor of Civil Engineering, Rajeev Gandhi Memorial College of Engineering and Technology, Nandyal, A.P, INDIA.**

drchenna78@gmail.com, Contact No: +91 90323 45197

Abstract:

This paper investigates the Constant Ductility Displacement Response Spectra (CDDRS) for near-fault ground motions (NFGM) of the 1999 Chi-Chi earthquake. The complex source mechanism was mainly caused by a rupture on the Chelungpu fault that spanned about 100 kilometres. In order to comprehend, a dataset of sixty three NFGM records have been considered to understand the effects of CDDRS due to hanging wall, foot wall, and directivity effects. The CDDRS are generated using SEISMO SIGNAL tool for the selected ground motions. Significant variation is observed in both elastic and inelastic CDDRS for tall buildings due to hanging wall effect. In addition, the variations in inelastic spectra are found to be more prominent due to backward directivity effect. Moreover, the inelastic displacement spectra values for pulse-like

ground motions are much higher than the spectra values associated with non-pulse ground motions.

Keywords: Taiwan; near-fault ground motions; constant ductility response spectra; seismic hazard

Introduction

The 1999 Chi-Chi earthquake (921 earthquake), which was one of the greatest reverse fault earthquakes, occurred in the seismically active area of Taiwan at a depth of 7 km, along the Chelungpu fault, caused by the collision of the Eurasian and Philippine sea plates[1]. The data from recent earthquakes has shown that the ground motion records in the near-fault (NF) region are quite distinct from those obtained from far-field regions[2]. The near-fault ground motion records contain most of the energy in a single or few pulses. Such intense concentration of energy can cause enormous structural damage. The preliminary investigation indicates that around 3000 buildings were collapsed and 6000 buildings were partially damaged during the earthquake[3,4]. In addition to buildings, other structures like bridges, dams, railways, and highways were also suffered severe damage during the earthquake[5]. Damage incurred by several cities adjacent to the fault and the number of buildings affected by the type of structure is depicted in figure 1. Severe damage took place to structures along the length of the fault during the earthquake. The Chelungpu fault trace passed beneath the building in Wu-Feng as shown in figure 1. This rupture produced a vertical displacement of about 2 m through the building. The building was severely damaged due to the differential movement of the fault trace. Another spectacular structural failure is the famous Shihkang dam which was directly uplifted by the fault trace[6]. It was offset by approximately 10 m near its right abutment, primarily due to the dip-slip fault rupture.

In the recent years, displacement-based seismic design has been increasingly implemented as compared to the traditional lateral forces design. Here, the CDDRS plays a crucial role for evaluation of the preliminary design of new structures. Several researchers have examined the influence of ductility requirements for engineering structures under earthquakes[7-11]. Freeman originally developed the Capacity Spectrum Method (CSM) in 1970s, and later Newmark presented the idea of an inelastic response spectrum based on elastic spectra for single-degree-of-freedom systems (SDOF)[10]. Reduction factors were introduced for developing inelastic response spectra for the ground motions from the 1940 El-Centro and 1952 Taft earthquakes[12,13]. Response Reduction Factors (R) were derived for the behavior of strength and stiffness degrading systems[14,15]. The ductility ratio, the period of the structure, and the site conditions were found to have a significant impact on the response spectra[16]. The impact of soil conditions was not thoroughly studied until 1990. Later, the influence of inelastic strength requirements of SDOF considering soil conditions was examined for various ground motion records[17]. Over the years, several empirical equations have been proposed using the constant ductility spectra or damage spectra for the Inelastic Displacement Ratio (IDR), but these studies did not consider pulse-like (PL) ground motions. A recent study performed on the evaluation of constant damage IDR with PL ground motions indicates that these represent greater hazard for structures with strength-degrading behavior[18]. The modern shift towards performance-based earthquake engineering emphasizes strongly the crucial importance of inelastic response spectrum for both SDOF and MDOF systems under PL ground motions[19, 20]. Large pulse period and peak ground velocity greatly increase the inelastic displacement, velocity, and acceleration spectra, indicating that the inelastic response spectra are sensitive to ground motion characteristics and structural hysteresis behavior[21]. Further, to account for the impact of the soil classification and focal mechanism, the study suggests an elastic displacement response spectrum

methodology for near-fault ground motions, that can be used in seismic design since they closely resemble the average elastic displacement response spectra of real earthquake[22]. A constant ductility energy factor spectra were introduced using Gauss–Newton technique for both near and far-fault ground motions[23]. It is shown that significant correlation exists between the computed and estimated energy constant-ductility energy factor spectra. The design of structures as per the contemporary displacement-based methods requires the displacement response spectra for ground motions at the site of interest. Under severe ground motions, the behavior of the structure is inelastic in nature, thus understanding the spectral properties for ductile systems are essential. The structure can be seismically designed to achieve sufficient strength as per these constant ductility response spectra.

The examination of literature indicated that the CDDRS have not been critically examined for NFGMs under various site geology conditions. A key reason could be the limited availability of ground motion records. Since the characteristics of NFGMs are strongly influenced by source rupture processes, they vary significantly from far-field ground motions. Hence, it is essential to examine their constant ductility spectra which can offer insights based on the observed variations from elastic spectra, for various ductility ratios. The main objective of the present study is to investigate the inelastic spectral displacements for various ductility ratios ranging from 1.5 to 3.0 at an interval of 0.5 under NFGMs of the 1999 Chi-Chi earthquake. The study examines the displacement response spectra due to near-fault characteristics and velocity pulses. The study also comprises the variation of CDDRS with respect to site geological conditions.

Strong Motion Dataset of Taiwan

A Peak Ground Acceleration (PGA) of larger than 1 g was recorded on the southern part of the hanging wall and the PGA was gradually decreased to 0.5 g towards the north. Unusually large

values of Peak Ground Velocity (PGV) were also recorded: TCU068 station had a PGV of 383 cm/s and TCU052 station had a PGV of 254 cm/s. The ground motions were recorded at over 150 locations on the hanging wall and 340 locations on the footwall of the Chelungpu fault. In this study, a strong ground motion dataset of 63 NF seismic stations, within 20 km of the Chelungpu fault are collected from the Consortium of Organizations for Strong-Motion Observation Systems (COSMOS) for the 1999 Chi-Chi earthquake. Further, the ground motions are classified according to forward rupture directivity, backward rupture directivity, hanging wall effect and foot wall effect, out of which 6 stations are located on the hanging wall, and 57 stations are located on the footwall as shown in table 1. Figure 2 shows the geographic locations of seismic stations used in the analysis. The site geology of soil is classified according to the National Earthquake Hazards Reduction Program (NEHRP) guidelines based on shear wave velocity at top 30 m. Around 42 sites possess stiff soils in the top 30 m with $V_{s,30}$ varies within 180-360 m/s and 3 sites possess soft soil with $V_{s,30}$ is less than 180 m/s. The amplification factors are high (2.5-2.7) for the sites TCU065 and TCU072 located 10 km apart from the fault. In addition, resonant phenomenon in subsurface soils was observed for the sites located in the NF zones of the 1999 Chi-Chi earthquake.

Methodology to Construct Constant Ductility Displacement Response Spectrum

The current section briefly discusses the methodology to construct the CDDRS for elasto-plastic systems consistent with various levels of the ductility ratio[24-26]. The schematic diagram is shown in figure 3. A step-by-step procedure is described below.

Step-1: The accelerogram $\ddot{u}_g(t)$ is numerically defined.

Step-2: Select the damping ratio, ξ and fundamental natural time period, T_n.

Step-3: Identify the linear system's response *u(t)* and select peak response $u_o(t)$. Calculate the peak force $f_o = ku_o$.

Step-4: Find the elasto-plastic system's response *u(t)*for the same time period and damping ratio. Calculate the yield force, $f_y = \bar{f}_y f_o$ for a range of values ($\bar{f}_y$ = 0.5, 0.25, 0.125). Find the maximum deformation u_m and the corresponding ductility factor (μ) from *u(t)*. Repeat the analysis using other values of $\bar{f}_y$ and, μ.

Step-5: Determine the value, $\bar{f}_y$, for the selected μ, using the results of step-4. If more than one $\bar{f}_y$ value corresponds to a specific value of μ, the largest value of $\bar{f}_y$ is chosen.

Step-6: The spectrum appropriate for the value selected in step 5 is produced by repeating steps 2 through 5 over a range of time periods.

Step-7: For various values of μ, repeat steps 2 through 6.

The analysis considers the displacement ductility μ values ranging from 1.5 to 3.0 with an interval of 0.5, as the typical ranges of μ are in between 3.0 and 6.0[27]. In this analysis, the recently proposed Pulse Indicator (PI) by Kardoutsou is used for classification of PL and NPL ground motions[22]. The results will change if other PI are used for the analysis, as the PI formulation differs for other authors. The PI is characterized based on cross-correlation factor (r) and the equation is as follows.

$$r = \frac{\sum_i \left(f(t_i) - \tilde{f}\right) \mathrm{x}\, g(t_i - t_d) - \tilde{g}}{\left[\sum_i \left(f(t_i) - \tilde{f}\right)^2\right] \mathrm{x} \left[\sum_i \left(g(t_i - t_d) - \tilde{g}\right)^2\right]} \quad (1)$$

Where $\tilde{f}$ and $\tilde{g}$ being the mean values of the functions *f* and *g*, respectively. t_d is the time delay parameter at which the pulse starts.

Results and Discussion

585 **Characteristics of Near-Fault Ground Motions**

586 Large pulse amplitude and long pulse duration are the key features in the velocity records of
587 NFGMs. These observations are substantially different from far-field ground motions as
588 illustrated in figure 4. Further, most of the energy content is confined in a single or a few pulses.
589 These pulses can also be due to the *directivity effect* and the *fling effect*. In this section, CDDRS
590 are examined for hanging wall, footwall, forward and backward rupture directivity for various
591 ductility ratios (μ = 1.5, 2.0, 2.5, 3.0) are shown in figure 5. As, the spectral displacements vary
592 for each ground motion record at a particular fundamental period of the structure, it is essential
593 to use the mean values. Further, the ground motions are classified as either PL or NPL using
594 different schemes, to evaluate the CDDRS for obtaining the structural response.

595 ***Hanging wall:*** A set of six stations are situated on the hanging wall side of the Chelungpu
596 fault. The spectra of ground motions from these stations, for various ductility ratios, are
597 compared with the elastic displacement spectrum. A variation is observed between inelastic
598 spectra of different ductility ratios. No significant variation is observed between the elastic and
599 the inelastic spectra till T_n reaches 2.35 s. and significant variation is observed beyond T_n = 2.35
600 s (i.e., for tall buildings).

601 ***Footwall:*** A set of fifty-seven stations are situated on the footwall side of the Chelungpu
602 fault. The spectra of ground motions from these stations, for various ductility ratios, are
603 compared with the elastic displacement spectrum. It has been observed that there is insignificant
604 variation between inelastic displacement spectra of various ductility ratios and the elastic
605 displacement spectrum on footwall.

606 ***Forward rupture directivity:*** A set of fifty-three stations are located on the forward rupture
607 directivity side of the Chelungpu fault. The spectra of ground motions from these stations, for
608 various ductility ratios, are compared with the elastic displacement spectrum. There is no

609 significant variation in the inelastic spectra obtained for different ductility ratios and the elastic
610 spectrum. It indicates that the forward rupture directivity has no substantial effect on the elastic
611 and the inelastic displacement spectra.

612 ***Backward rupture directivity:*** A set of ten stations are located on the backward rupture
613 directivity side of the Chelungpu fault. The spectra of these stations, for various ductility ratios,
614 are compared with the elastic displacement spectrum. It is observed that there is a significant
615 variation between the inelastic spectra of different ductility ratios and the elastic spectrum. No
616 significant difference is observed between inelastic spectra with various ductility ratios. The
617 average elastic and inelastic spectra for various ductility ratios are shown in figure 6.

618

619 **Velocity Pulse Parameters**

620 The ground motion records are classified as *PL*, *NPL* and *ambiguous* using the approach
621 proposed by Kardoutsou[28]. The current study uses Kardoutsou PI for pulse classification.
622 According to this approach, if the PI values are greater than 0.65 the ground motions are termed
623 as *PL*. If PI is less than 0.55, such ground motions are termed as *NPL*. If the value of PI lies
624 between 0.55 and 0.65, the ground motions are termed as *ambiguous.* A sharp velocity pulses
625 exhibit high amplitude and long pulse duration may lead to significant damage to engineered
626 structures. The current study examines the effect of pulse period and pulse identification on
627 CDDRS.

628 ***Pulse period:*** Four different pulse periods 1.2 s, 1.8 s, 3.3 s, and 3.9 s are considered for the
629 study. No substantial change in inelastic response spectra is observed for the fundamental time
630 period, T<1.3 s and significant change is observed beyond T=1.3 s. This indicates that the
631 velocity pulse periods can influence the inelastic response spectra for high-rise buildings. Figure
632 7 shows the inelastic displacement spectra.

Pulse identification: The inelastic displacement spectra are drawn for ductility ratios of 1.5, 2.0, 2.5, and 3.0. Since the ground motion data is large, an average inelastic spectrum is considered for all μ values. It is observed that the inelastic displacement spectra values for PL ground motions are twice the values observed for NPL ground motions. No significant deviation is observed in the inelastic displacement spectra of PL and NPL ground motions for various ductility values shown in figure 7. However, a deviation is observed in ambiguous ground motions for T > 2.5 s. The results may vary with other definitions of PI. For this purpose, a comparison has also been performed using other PIs proposed by various authors. Figure 8 represents the inelastic displacement spectra for PL, and NPL proposed by various researchers for ductility ratio $\mu = 3.0$[29-31, 27]. It is observed that the PL spectra, based on Baker and Panella PI's, lead to higher inelastic spectral displacements due to a higher PI values defined by both researchers. According to Baker and Panella, the PL ground motions are those for which the PI values are greater than 0.85, and 0.7, respectively. It is also observed that the NPL spectra based on Baker's PI, lead to lower displacement values. These observations indicate the importance of PL and NPL ground motions for developing CDDRS.

Effect of Closest Distance from the fault, R

Various distances: To study the inelastic displacement response spectra for various closest distances from the fault, a plot is drawn as shown in figure 9. High displacement values are observed for the closest distance to fault, R=1.1 km till T < 2.3 s. No significant change is observed in spectra for T < 2.3 s for higher distance values. Beyond this range, the displacement values are considerably high.

Same distance: Two seismic stations located at the same closest distance to the fault, i.e.13.3 km are examined. While one station is situated on a hanging wall, the other station is situated on the footwall. The inelastic displacement spectra are developed for ground motions

from the two stations with different ductility ratios. From the results, it is observed that the station located on the hanging wall leads to larger displacement values as compared to the station located on the footwall, as shown in figure 9. In the case of hanging walls, the seismic energy gets trapped on the wedge portion resulting in higher acceleration values.

Effect of site classification

In the 1999 Chi-Chi earthquake, most recording stations were situated on soil. The soil behavior was non-linear in the NF region[32]. Since detailed borelog data and subsurface soil properties are often not available for every site, sites are usually classified into various classes, using information from a combination of sources, i.e. geological maps, digital elevation models, borelog data, shear wave velocity and response spectra from historical ground motion data. The site class description used in the present study is based on geological studies of the region reported by Lee[33].

From figure 10, no significant change is observed in inelastic displacement spectra for various μ values for T_n is less than 1.0 s (for low-rise and mid-rise buildings) and considerable change is observed for T_n beyond 1.0 s. For higher site classification, the inelastic displacement values change abnormally for T_n beyond 1.0 s due to nonlinearity of soil. Overall, the results obtained from various site classifications indicate the NFGMs have a distinct impact in the various CDRS. The results thereby provide an insight into the general evaluation of CDDRS for NFGMs.

CDDRS with different authors

A comparison is done between CDDRS obtained from the *Seismosignal* and *Open Seismo MATLAB* application tools for validation purposes[34, 35]. The present study uses the commercial *Seismosignal* tool for developing CDDRS at four seismic stations WNT, CHY028, CHY080,

TCU065 that are located 2.2 km, 8.7 km, 3.1 km, 2.5 km from the Chelungpu fault respectively. A key reason for the selection of the tool is that it is an easy to use, reliable and the most widely used tool by various researchers worldwide. For the purpose of validation, the derived results are compared with the *Open-Seismo MATLAB* tool developed by George Papazafeiropoulas[36]. It is known that conventional time integration algorithms are incorporated in *Seismosignal* to calculate the dynamic response. However, the *Open-Seismo MATLAB* tool computed the CDDRS through nonlinear dynamic analyses of elasto-plastic hysteretic systems, rather than simplified approaches. The target ductility $\mu = 3.0$ is considered in the analysis. No significant change in inelastic spectra is observed using both application tools. A slight variation is observed for the station CHY028 at periods between fundamental natural periods T = 2.25 s and 3.0 s. Though the percentage of error is negligible, a slight variation is observed between spectra using both application tools as shown in figure 11. The variation in the results is due to the following:

- *Seismosignal* tool uses conventional time integration algorithms and *Open-Seismo MATLAB* uses advanced time integration algorithms to minimize the errors for certain cases.
- Elasto-plastic bilinear kinematic hardening constitutive models for Single Degree of Freedom (SDOF) systems are implemented in *Open-Seismo MATLAB.*
- *Open-Seismo MATLAB* uses Generalized Single Step Single Solve (GSSSS) algorithms for calculating the displacement of the SDOF systems and *Seismosignal* tool uses Newmark's family algorithms.

Conclusions

The structural damage in near-fault regions was high and it was reported that unreinforced masonry structures and reinforced concrete structures were destroyed in Taichung and Nantou during the 1999 Chi-Chi earthquake. Literature on constant ductility spectra for near-fault

ground motions is limited due to scarcity of near-fault data recorded in major earthquakes. The current study presents CDDRS from various ground motion records of the 1999 Chi-Chi earthquake due to near-fault characteristics. Some salient conclusions are now discussed.

- The elastic and inelastic CDDRS have no remarkable effect across all periods of buildings due to the ground motions located on foot wall of the Chelungpu fault. On other hand, significant variations are observed in both elastic and inelastic CDDRS for tall buildings (T_n> 2.35 s) due to hanging wall effect. Reconnaissance studies also indicate that greater structural damage was observed on the hanging wall side.
- Notable changes are observed in the inelastic CDDRS due to backward rupture directivity, but no effect is observed on the CDDRS due to forward rupture directivity.
- Inelastic CDDRS for PL ground motions are twice than NPL ground motions due to large amplitude and period of ground motions.
- Further, the results obtained from various site classifications indicate the near-fault ground motions have a significant and distinct impact in the CDRS. Both low-rise and mid-rise buildings, no significant change are observed in the inelastic CDRS for different ductility values of mid-rise buildings (T_n< 1.0 s), and significant variation is observed for high-rise buildings (T_n> 1.0 s).
- Finally the results are validated using two softwares and it is observed that the results are to be within a reasonable level of accuracy.

The CDDRS evaluation does not incorporate the influence arising from the various orientations of ground motion records.

Conflict of Interest

The author(s) declare that there is no conflict of interest regarding this article's research, authorship, and/or publication.

References

37. Shin, T.C. and Teng, T.L., An overview of the 1999 Chi-Chi, Taiwan, earthquake. *Bulletin of the seismological society of America*, 2001, **91**(5), 895-913.
38. Alavi, B. and Helmut, K., Effects of near-fault ground motions on frame structures. Stanford: John A. Blume Earthquake Engineering Center, USA, 2001.
39. Chen, C. C. Huang, C. T. Cherng, R. H. and Jeng, V., Preliminary investigation of damage to near fault buildings of the 1999 Chi-Chi earthquake. *Earthquake Engineering and Engineering Seismology*, 2000, **2**(1), 79-92.
40. Tsai, K. C. Hsiao, C. P. and Bruneau, M., Overview of building damages in 921 Chi-Chi earthquake. *Earthquake Engineering and Engineering Seismology*, 2000, **2**(1), 93-108.
41. Su, N. Lin, T. D. and Chai, H. W., Damage to structures and buildings from the Chi-Chi (Taiwan) earthquake. *Proceedings of the Institution of Civil Engineers-Structures and Buildings*, 2002, **152**(1), 51-56.
42. Bray, J.D., Developing Mitigation Measures for the Hazards Associated with Earthquake Surface Fault Rupture, *Seismic Fault-induced Failures*, 2001, 55-80.
43. Veletsos, A. S. Newmark, N. M. and Chelapati, C. V., Deformation spectra for elastic and elastoplastic systems subjected to ground shock and earthquake motions. *Proc. 3rd world conference on earthquake engineering, NewZealand*, 1965, 663-682.
44. Newmark, N. M. and Hall, W. J., Seismic design criteria for nuclear reactor facilities. *Proc. 4th World conference on Earthquake Engineering, Santiago*, 1969, 37-50.

45. Murakami, M. and Penzien, J., Nonlinear response spectra for probabilistic design of reinforced concrete structures. *Proc. 6th World Conference on Earthquake Engineering, New Delhi*, 1977, 1046-1051.
46. Newmark, N. M. and Riddle, R., Inelastic spectra for seismic design. *Proc. 7thWorld Conference on Earthquake Engineering, Istanbul*, 1980, 129-136.
47. Lai, S. S. P. and Biggs, J. M., Inelastic response spectra for aseismic building design. *Journal of the Structural Division*, 1980, **106**(6), 1295-1310.
48. Saini, S. S., Design spectrum for epicentral earthquakes. *Proc. 2nd International Conference on Computer Aided Analysis and Design in Civil Engineering, University of Roorkee, India*, 1985, 41-47.
49. Pal, S. Dasaka, S. S. and Jain, A. K., Inelastic response spectra. *Computers and structures*, 1987, **25**(3), 335-344.
50. Riddell, R. Hidalgo, P. and Cruz, E., Response modification factors for earthquake resistant design of short period buildings. *Earthquake spectra*, 1989, **5**(3), 571-590.
51. Krawlinker, H. and Nassar, A., Seismic design based on ductility and cumulative damage demands and capacities. In: Nonlinear seismic analysis of reinforced concrete buildings. CRC Press, New York, USA, 1992, 27–47.
52. Chopra, A. K. and Goel, R. K., Capacity-demand-diagram methods based on inelastic design spectrum. *Earthquake Spectra*, 1999, **15**(4), 637-656.
53. Miranda, E., Nonlinear response spectra for earthquake resistant design. *Proc. 10th World Conference on Earthquake Engineering*, Madrid, Spain. 1992.
54. Wei-Ping, W. Chang-Hai, Z. Shuang, L. Zhiwang, C. Li-Li, X., Constant damage inelastic displacement ratios for the near-fault pulse-like ground motions, *Engineering Structures*, 2014, **59**, 599-607.

55. Changhai, Z. Weiping, W. Duofa, J. Shuang, L., The influences of aftershocks on the constant damage inelastic displacement ratio. *Soil Dynamics and Earthquake Engineering*, 2015, **79,** 186-189.

56. Foteini, K. George, H., Constant-ductility inelastic displacement, velocity and acceleration ratios for systems subjected to simple pulses, *Soil Dynamics and Earthquake Engineering*, 2020, **131,** 106027.

57. Dong, H. Han, Q. Du, X. Cheng, S. He, H., Inelastic response spectra of self-centering structures with the flag-shaped hysteretic response subjected to near-fault pulse-type ground motions. *Earthquake Spectra*. 2021, **37**, 2767-2794.

58. Maniatakis, C.A. Spyrakos, C.C., A new methodology to determine elastic displacement spectra in the near-fault region. *Soil Dynamics and Earthquake Engineering*, 2012, **35**, 41-58.

59. Ucar, T. Merter, O., Predictive Model for Constant-Ductility Energy Factor Spectra of Near- and Far-Fault Ground Motions Based on Gauss–Newton Algorithm. *Journal of Earthquake Engineering*, 2022, **15**, 7689-7714.

60. Yi, W.J. Zhang, H.Y. Kunnath, S.K. Probabilistic constant-strength ductility demand spectra. *Journal of structural engineering*, 2007, **133**, 567-575.

61. Colunga, A.T., Displacement ductility demand spectra for the seismic evaluation of structures. *Engineering Structures*, 2001, **23**, 1319-1330.

62. Madhu, G.H. Gupta, V.K., Scaling of constant-ductility residual displacement spectrum. *Earthquake Engineering & Structural Dynamics*, 2020, **49**, 215-233.

63. Alfredo, R.S. Edén, B. Juan, B. Federico, V.B. Mario, D. and Llanes, T., Energy Dissipation and Local, Story, and Global Ductility Reduction Factors in Steel Frames under Vibrations Produced by Earthquakes, *Shock and Vibration*, 2018, 9713685.

64. Kardoutsou, V. Taflampas, I. and Psycharis, I. N., A new pulse indicator for the classification of ground motions. *Bulletin of the Seismological Society of America*, 2017, **107**(3), 1356-1364.
65. Baker, J. W., Quantitative classification of near-fault ground motions using wavelet analysis. *Bulletin of the seismological society of America*, 2007, **97**(5), 1486-1501.
66. Panella, D. S. Tornello, M. E. and Frau, C. D., A simple and intuitive procedure to identify pulse-like ground motions. *Soil Dynamics and Earthquake Engineering*, 2017, **94**, 234-243.
67. Zhai, C. Chang, Z. Li, S. Chen, Z. and Xie, L., Quantitative identification of near-fault pulse-like ground motions based on energy. *Bulletin of the Seismological Society of America*, 2013, **103**(5), 2591-2603.
68. Pavlenko, O.V., Characteristics of soil response in near-fault zones during the 1999 Chi-Chi, Taiwan, Earthquake. *Pure and applied geophysics*, 2008, **165**(9), 1789-1812.
69. Lee, C.T. Cheng, C.T. Liao, C.W. and Tsai, Y.B., Site classification of Taiwan free-field strong-motion stations. *Bulletin of the Seismological Society of America*, 2001, **91**(5), 1283-1297.
70. SeismoSoft, Seismo Signal A computer program for signal processing of strong-motion data, Pavia, Italy, 2021.
71. The MathWorks, Inc., MATLAB Release 2020b Natick, Massachusetts, United States of America, 2020
72. Papazafeiropoulos, G. and Plevris, V., Openseismomatlab: A new open-source software for strong ground motion data processing. *Heliyon*, 2018, **4**(9), 784.

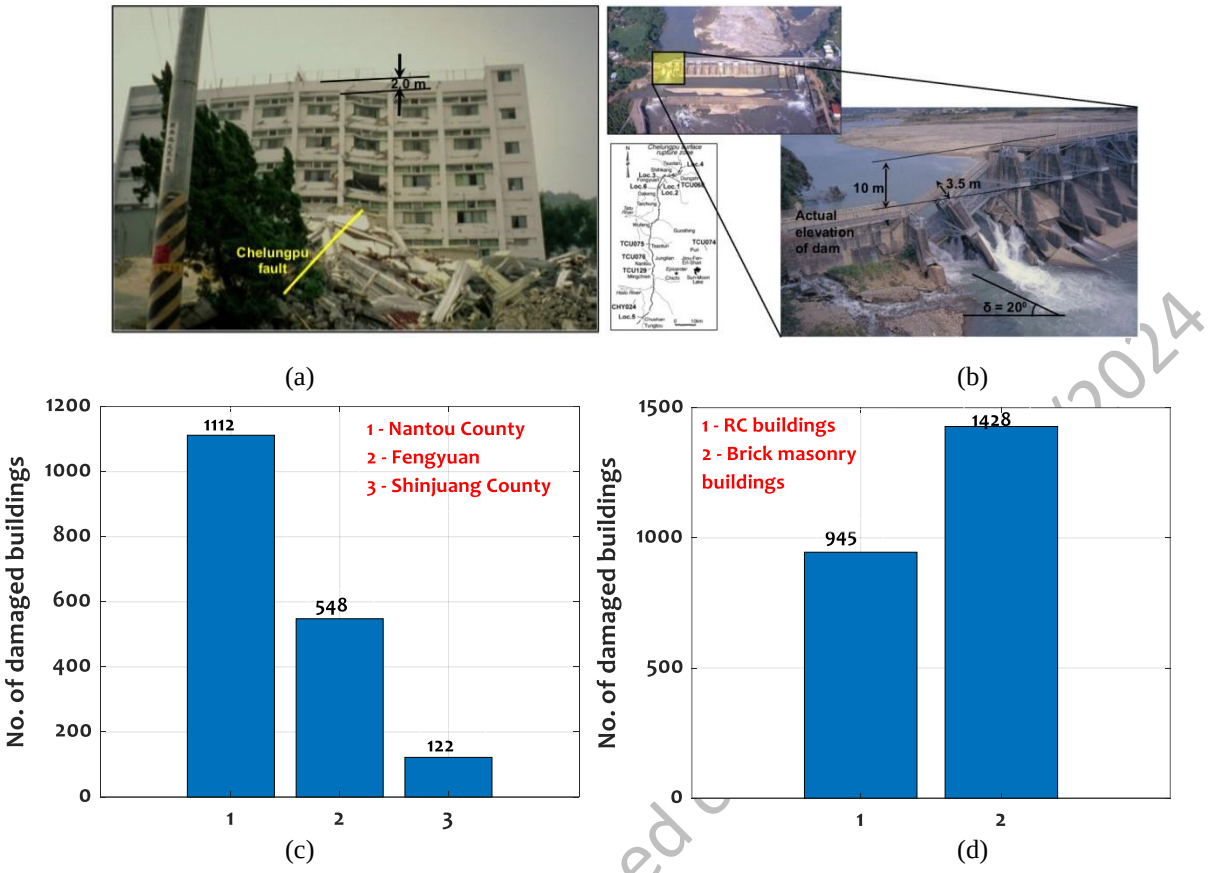

Figure 1. Damage of structures due to surface rupture and statistics of the damaged buildings in affected areas during 1999 Chi-Chi earthquake (a) the Chelungpu fault passed beneath this apartment building in Wu Feng (Photo Courtesy: K. Kelson). (b) view to the east of surface fault rupture through Shihkang Dam (Photo Courtesy: J.D. Bray). (c) number of damaged buildings in affected areas of Taiwan, and (d) number of damaged RC and brick masonry buildings.

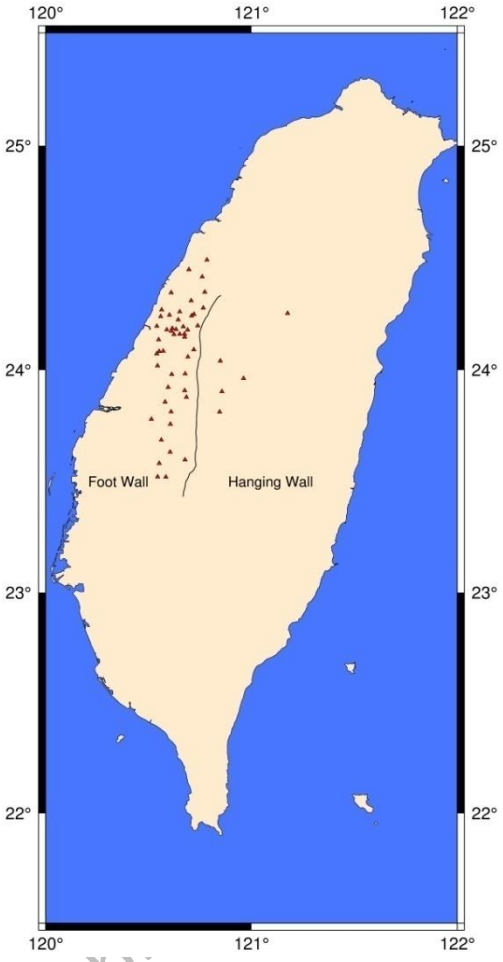

832

833 Figure 2. Location of seismic stations considered in the analysis

834

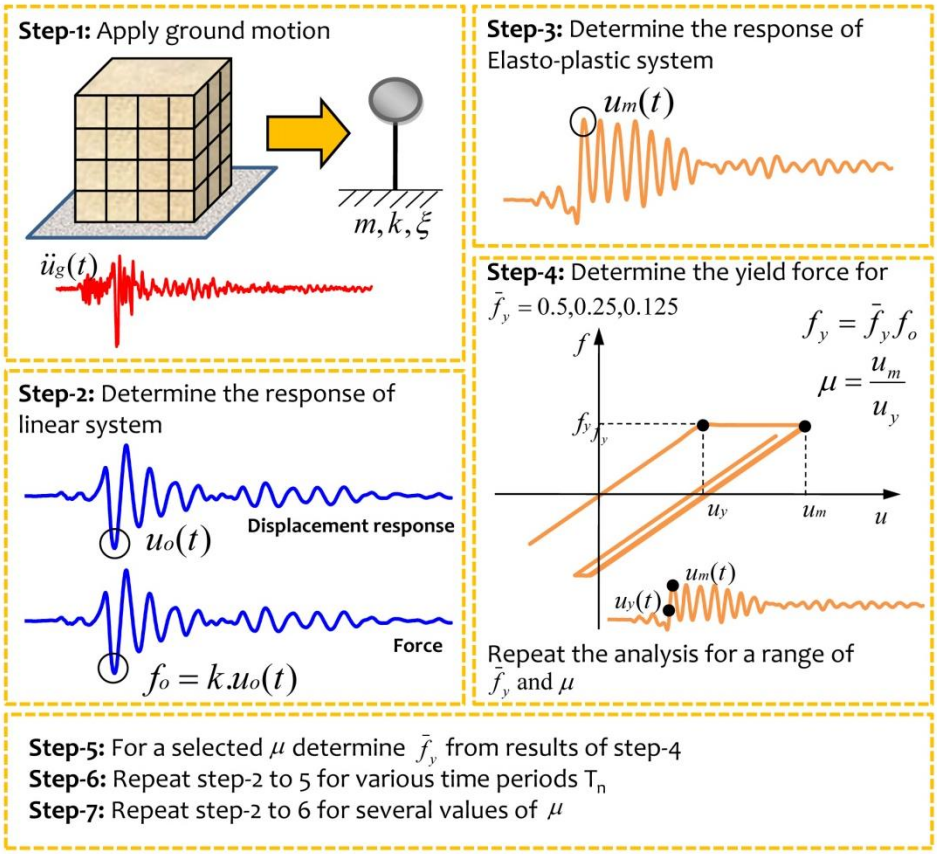

Figure 3. Schematic diagram of constructing constant ductility response spectrum

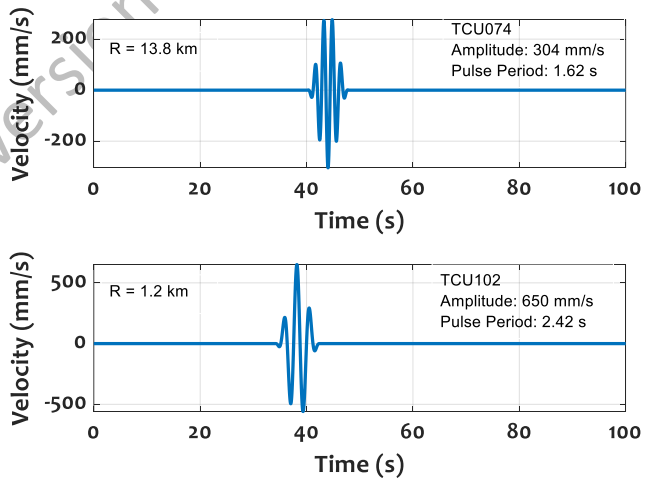

Figure 4. Velocity pulses at two different stations

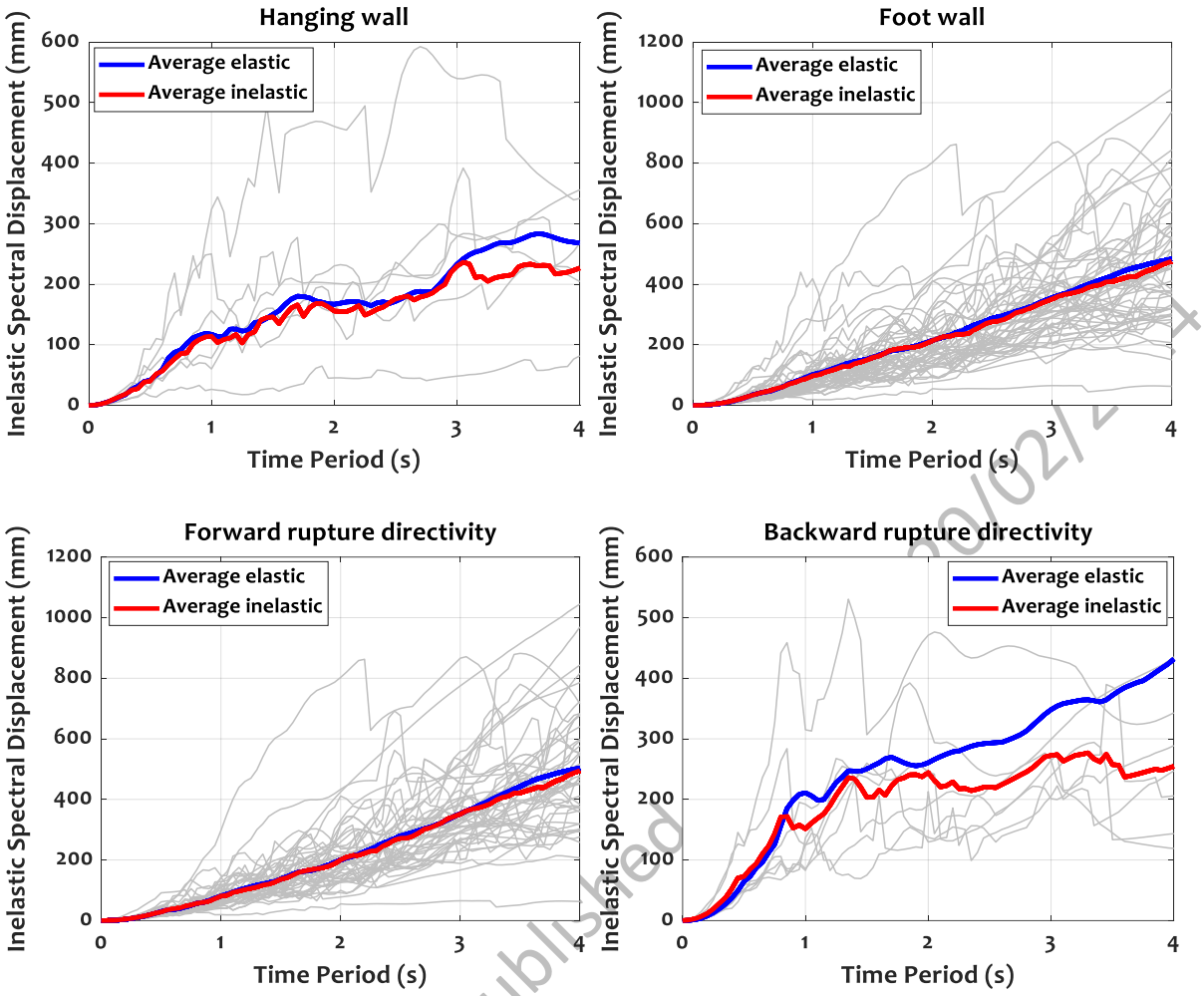

Figure 5. Inelastic spectral displacements for hanging wall, foot wall, forward and backward rupture directivity of near- fault ground motions during 1999 Chi-Chi earthquake (μ=3.0). The average elastic spectrum and inelastic spectrum are represented with blue and red colors respectively.

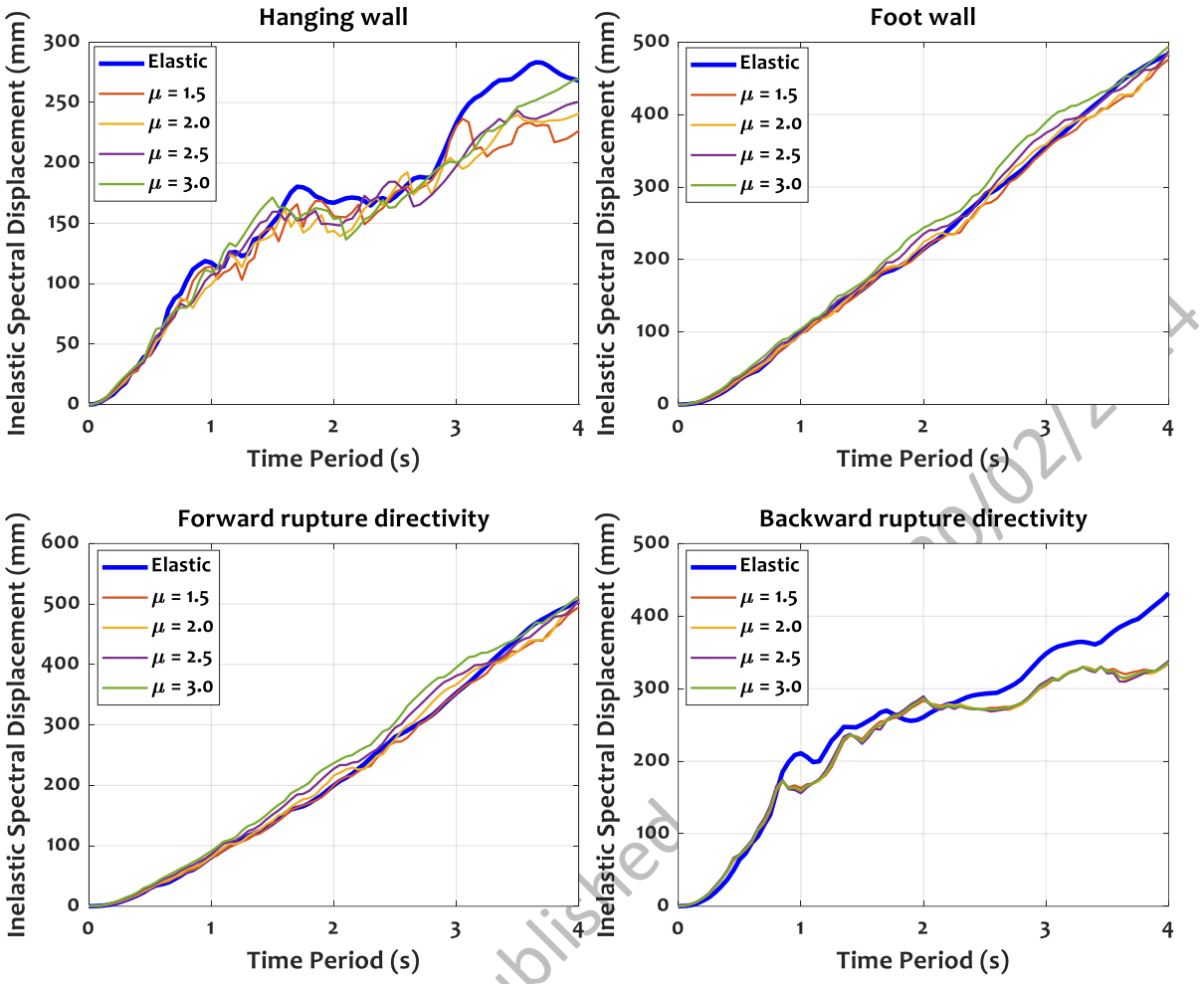

Figure 6. Mean of elastic and inelastic spectral displacements for different ductility ratios

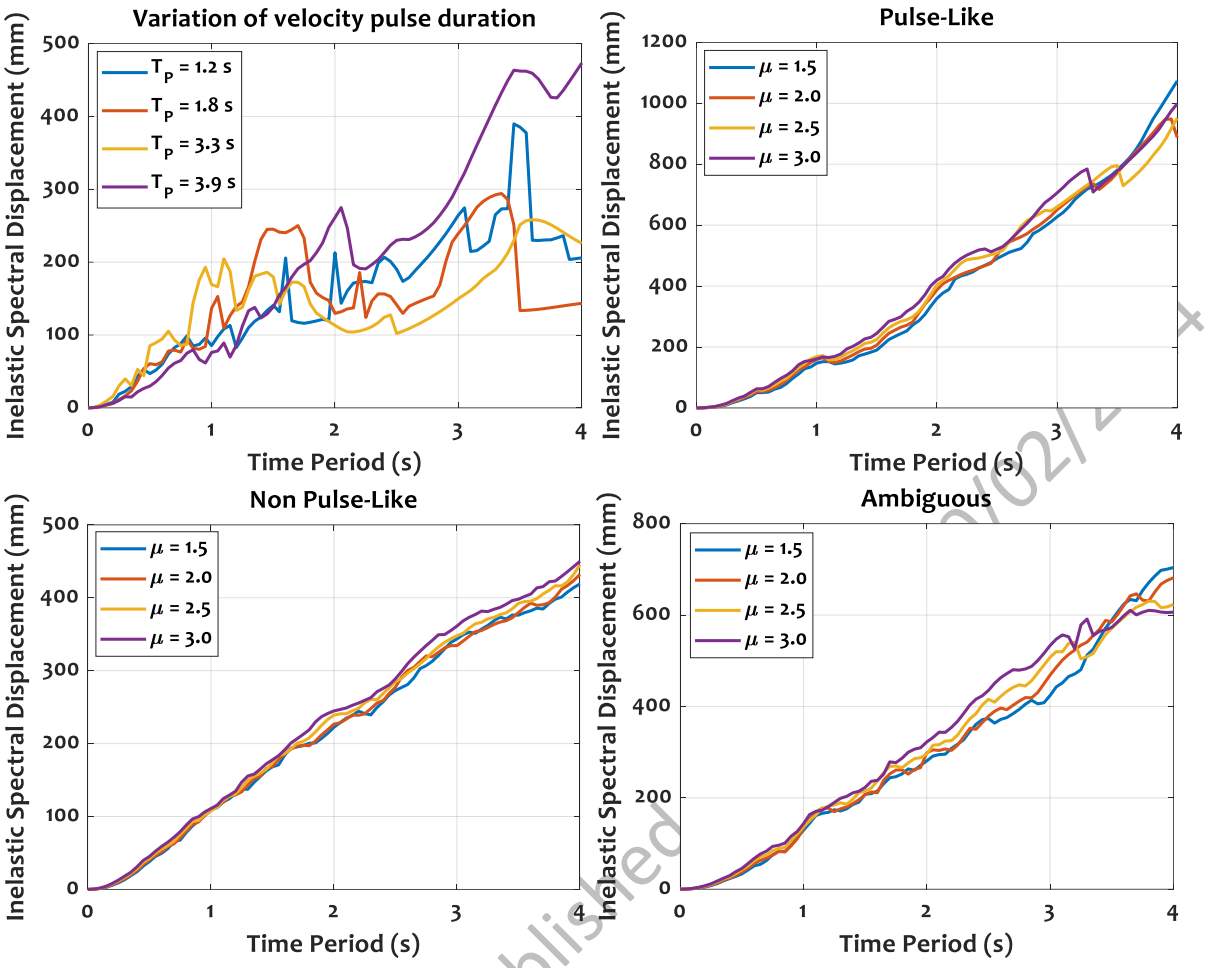

Figure 7. Comparison of displacement spectra for various pulse periods and various ductility ratios of pulse-like, non pulse-like, and ambiguous ground motions of the 1999 Chi-Chi earthquake.

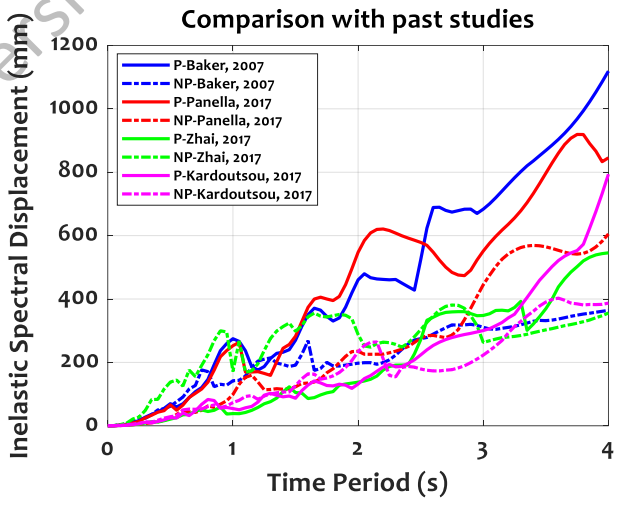

Figure 8. Classification of inelastic displacement spectra for pulse-like and non-pulse like ground motions defined by various researchers (μ=3.0). The current study uses Kardoutsou PI for pulse classification.

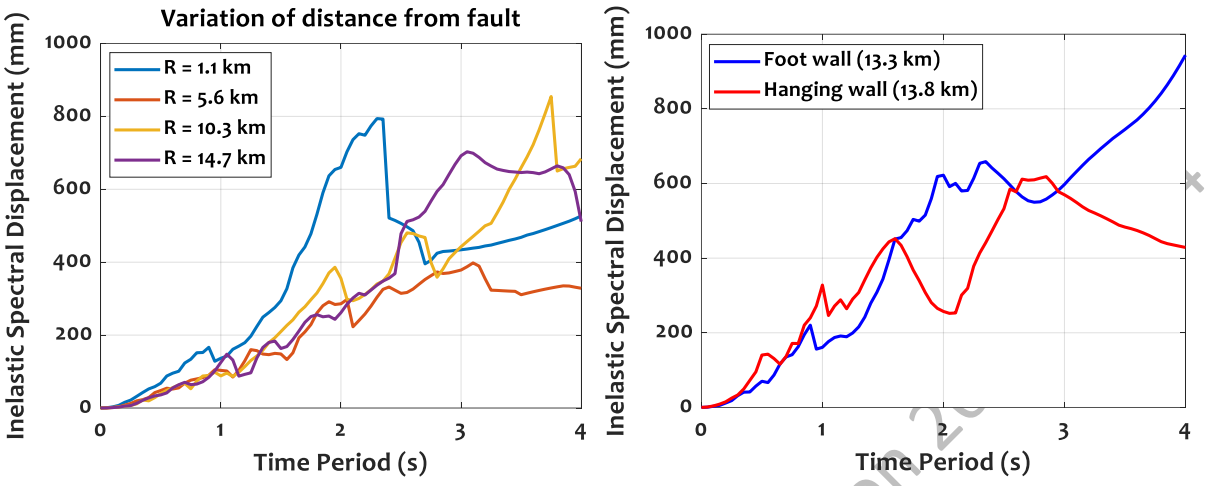

Figure 9. Comparison of inelastic displacement spectra with the stations located at different distances and same distance from fault (μ=3.0)

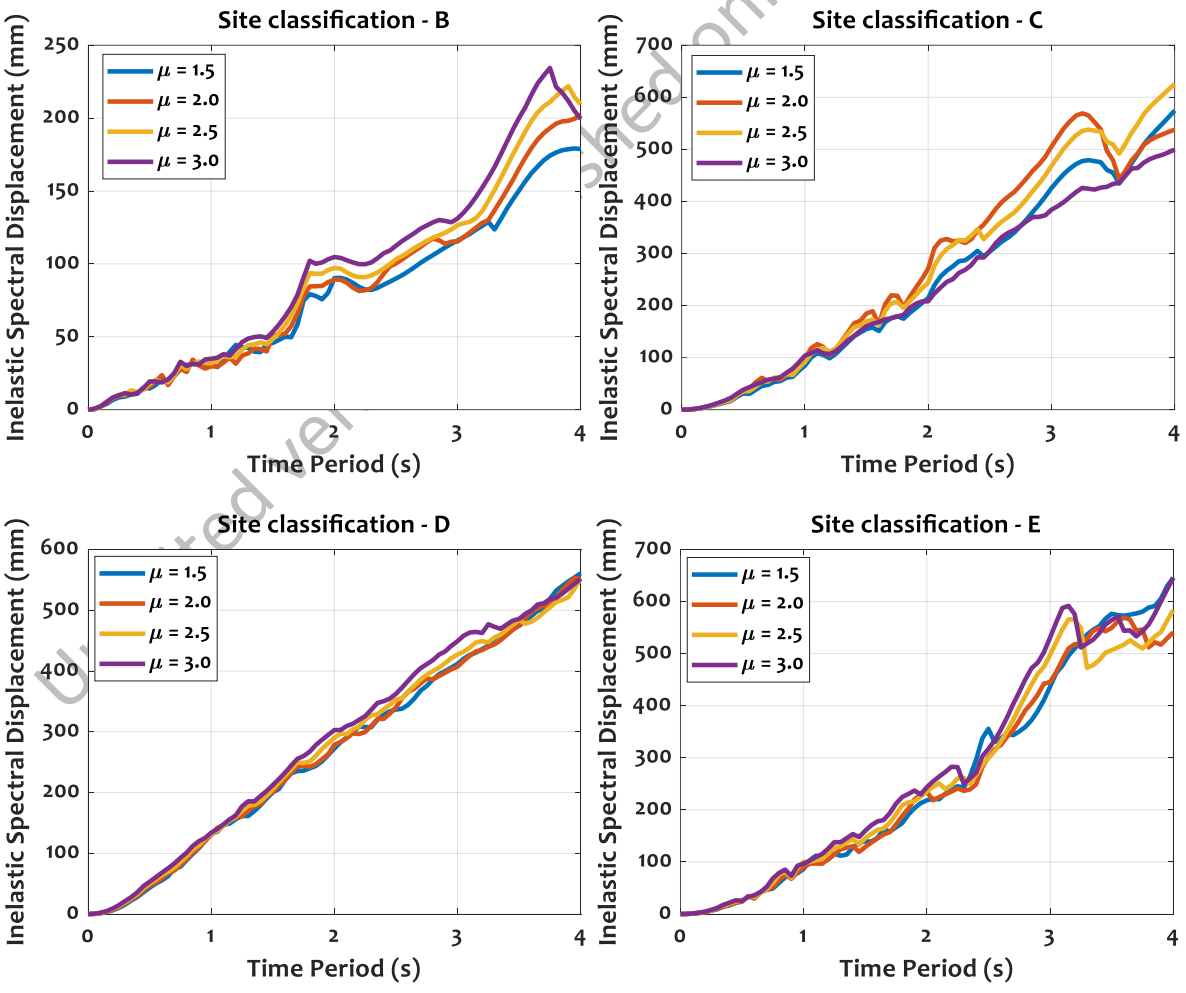

873 Figure 10. Comparison of inelastic displacement spectra with various site classifications B, C, D,
874 and E for various ductility ratios

875

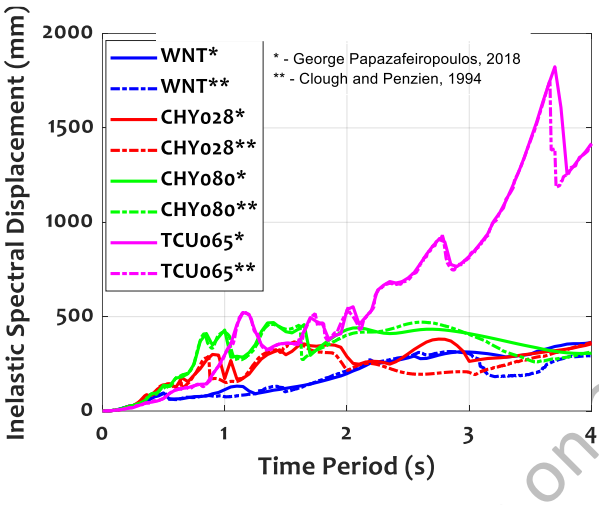

876

877 Figure 11. Comparison of inelastic displacement spectra with various methods proposed by
878 different authors

879

880

881

882

883 Table 1.Details of seismic stations of the 1999 Chi-Chi earthquake occurred on 20 September
884 1999 with a magnitude of Mw7.6 (latitude: 23.86, longitude: 120.80) *(Data Source: COSMOS)*

SNo	Station Name	Station Lat.	Station Long.	Closest Distance to Fault (km)	Epicentral Distance (km)	Site Geology	Near-Fault Characteristics			
							Hanging Wall	Foot Wall	Forward Rupture	Backward Rupture
1	TCU078	23.81	120.85	8.30	7.40	D	*		*	
2	TCU089	23.90	120.86	12.80	7.95	C	*		*	
3	WNT	23.88	120.68	2.20	12.94	D		*	*	
4	TCU076	23.91	120.68	3.20	14.71	D		*	*	
5	TCU075	23.98	120.68	3.40	19.16	D		*	*	
6	TCU122	23.81	120.61	9.20	21.72	D		*	*	
7	TCU074	23.96	120.96	13.80	21.27	D	*		*	
8	TCU072	24.04	120.85	7.90	20.76	D	*		*	
9	TCU138	23.92	120.60	11.30	23.67	D		*	*	
10	TCU116	23.86	120.58	12.50	24.33	E		*	*	
11	CHY024	23.76	120.61	9.30	24.33	D		*	*	*
12	TCU120	23.98	120.61	9.90	24.62	C		*	*	
13	TCU065	24.06	120.69	2.50	25.10	D		*	*	
14	TCU067	24.09	120.72	1.10	27.11	D		*	*	
15	CHY025	23.78	120.51	18.80	32.97	E		*	*	
16	CSMIP	23.69	120.56	13.30	32.67	D		*		*
17	CHY101	23.69	120.56	13.30	32.67	D		*		*
18	TCU123	24.02	120.54	17.10	33.40	D		*	*	
19	CHY080	23.60	120.68	3.10	32.18	---		*		*
20	CHY028	23.63	120.61	8.70	33.28	D		*		*
21	TCU063	24.11	120.61	10.30	34.64	D		*	*	
22	TCU055	24.14	120.66	5.60	34.61	D		*	*	
23	TCU109	24.08	120.57	14.70	35.53	D		*	*	
24	TCU082	24.15	120.68	4.50	34.70	D		*	*	
25	TCU	24.15	120.68	4.50	34.70	D		*	*	
26	TCU106	24.08	120.55	16.70	37.00	D		*	*	
27	TCU107	24.07	120.54	17.80	37.21	D		*	*	
28	TCU054	24.16	120.68	4.60	36.15	D		*	*	
29	TCU051	24.16	120.65	7.00	37.12	D		*	*	
30	TCU049	24.18	120.69	3.30	37.40	D		*	*	
31	TCU056	24.16	120.62	9.80	38.45	D		*	*	
32	TCU052	24.20	120.74	1.80	38.08	D	*		*	
33	CHY074	23.51	120.80	14.40	38.88	C	*			*
34	CHY029	23.61	120.52	16.40	41.65	C		*		*

35	TCU053	24.19	120.67	5.50	39.73	D		*	*	
36	TCU050	24.18	120.63	8.90	40.12	D		*	*	
37	TCU057	24.17	120.61	11.20	40.56	C		*	*	
38	TCU061	24.14	120.55	17.20	41.31	D		*	*	
39	CHY006	23.58	120.55	14.50	41.38	D		*		*
40	TCU100	24.19	120.62	10.80	41.51	C		*	*	
41	TCU048	24.18	120.59	13.40	42.50	C		*	*	
42	TCU060	24.22	120.64	8.10	43.98	D		*	*	
43	TCU101	24.24	120.71	1.90	43.54	D		*	*	
44	CHY035	23.52	120.58	15.20	44.71	D		*		*
45	TCU102	24.25	120.72	1.20	44.05	D		*	*	
46	TCU070	24.20	120.54	18.40	47.08	C		*	*	
47	CHY034	23.52	120.54	18.20	47.11	D		*		*
48	TCU068	24.28	120.77	3.00	46.43	D		*	*	
49	TCU136	24.26	120.65	7.50	47.33	C		*	*	
50	TCU104	24.25	120.60	12.50	48.06	C		*	*	
51	TCU105	24.24	120.56	16.80	49.80	C		*	*	
52	TCU103	24.31	120.71	2.40	50.94	D		*	*	
53	TCU059	24.27	120.56	16.50	52.35	D		*	*	
54	TCU087	24.35	120.77	3.40	54.23	C		*	*	
55	TCU064	24.35	120.61	12.20	57.84	D		*	*	
56	TCU088	24.25	121.18	13.20	60.40	B	*		*	
57	NSY	24.42	120.76	9.10	61.86	C		*	*	
58	TCU128	24.42	120.76	9.10	61.86	C		*	*	
59	TCU036	24.45	120.70	12.70	66.32	D		*	*	
60	TCU040	24.45	120.64	15.00	67.78	E		*	*	
61	TCU046	24.46	120.85	16.50	66.80	B		*	*	
62	TCU039	24.49	120.78	17.50	70.11	C		*	*	
63	TCU038	24.49	120.66	18.20	71.59	D		*	*	

885

886